Protein Phosphatase 1 activity controls a balance between collective and single cell modes of migration

Yujun Chen[1], Nirupama Kotian[1], George Aranjuez[2,†], Lin Chen[3], C. Luke Messer[1], Ashley Burtscher[2], Ketki Sawant[1], Damien Ramel[3, §], Xiaobo Wang[3], and Jocelyn A. McDonald[1*]

[1]Division of Biology, Kansas State University, Manhattan, KS, USA

[2]Lerner Research Institute, Cleveland Clinic, Cleveland, OH, USA

[3]LBCMCP, Centre de Biologie Intégrative (CBI), Université de Toulouse, CNRS, UPS, Toulouse, France

[*]Author for correspondence: jmcdona@ksu.edu; Tel: +1 785-532-6087

[†]Present address: Division of Immunity and Pathogenesis, Burnett School of Biomedical Sciences, University of Central Florida College of Medicine, Orlando, Florida, USA

[§]Present address: Institute of Metabolic and Cardiovascular Diseases (I2MC), Université de Toulouse, Institut National de la Santé et de la Recherche Médicale (INSERM) UMR1048, Toulouse, France

Abstract

Collective cell migration is central to many developmental and pathological processes. However, the mechanisms that keep cell collectives together and coordinate movement of multiple cells are poorly understood. Using the *Drosophila* border cell migration model, we find that Protein phosphatase 1 (Pp1) activity controls collective cell cohesion and migration. Inhibition of Pp1 causes border cells to round up, dissociate, and move as single cells with altered motility. We present evidence that Pp1 promotes proper levels of cadherin-catenin complex proteins at cell-cell junctions within the cluster to keep border cells together. Pp1 further restricts actomyosin contractility to the cluster periphery rather than at internal cell-cell contacts. We show that the myosin phosphatase Pp1 complex, which inhibits non-muscle myosin-II (Myo-II) activity, coordinates border cell shape and cluster cohesion. Given the high conservation of Pp1 complexes, this study identifies Pp1 as a major regulator of collective versus single cell migration.

Introduction

Cells that migrate as collectives help establish and organize many tissues and organs in the embryo, yet also promote tumor invasion, dissemination and metastasis[1-5]. A wide variety of cells undergo collective cell migration during development, ranging from neural crest cells in *Xenopus*, the zebrafish lateral line primordium, and branching mammary glands[2,5-7], among many other examples. Despite the apparent diversity in collectively migrating cell types, there is remarkable conservation of the cellular and molecular mechanisms that underlie group cell movements. In particular, migrating collectives require fine-tuned organization and cell coordination to move effectively as a unified group. Similar to individually migrating cells, collectively migrating cells display a front-rear polarity, but this polarity is often organized at the group level[8]. Leader cells at the front extend characteristic protrusions that help collectives navigate tissues. Mechanical cell coupling and biochemical signals then reinforce collective polarity by actively repressing protrusions from follower cells and by maintaining lead cell protrusions that pull the group forward[8,9]. Importantly, cell-cell adhesions keep collectives together by maintaining strong but flexible connections between cells. Moreover, many cell collectives exhibit a "supracellular" organization of the cytoskeleton at the outer perimeter of the entire cell group that serves to further coordinate multicellular movement[7,10-12]. Despite progress in understanding how single cells become polarized and motile, less is known about the mechanisms that control the global organization, cohesion, and coordination of cells in migrating collectives.

Drosophila border cells are a genetically tractable and relatively simple model well-suited to investigate how cell collectives undergo polarized and cooperative migration within a developing tissue[13,14]. The *Drosophila* ovary is composed of strings of ovarioles made up of

59 developing egg chambers, the functional unit of the *Drosophila* ovary. During late oogenesis,
60 four to eight follicle cells are specified at the anterior end of the egg chamber to become
61 migratory border cells. The border cells then surround a specialized pair of follicle cells, the
62 polar cells, and delaminate as a multicellular cluster from the follicular epithelium.
63 Subsequently, the border cell cluster undergoes a stereotyped collective migration, moving
64 between 15 large germline-derived nurse cells to eventually reach the oocyte at the posterior end
65 of the egg chamber (Figure 1A-F). Throughout migration, individual border cells maintain
66 contacts with each other and with the central polar cells so that all cells move as a single
67 cohesive unit[15,16]. A leader cell at the front extends a migratory protrusion whereas protrusions
68 are suppressed in trailing follower cells[17-19]. As with other collectives, polarization of the border
69 cell cluster is critical for the ability to move together and in the correct direction, in this case
70 towards the oocyte (Figure 1A-F)[17,18].

71 Polarization of the border cell cluster begins when two receptor tyrosine kinases (RTKs)
72 expressed by border cells, PDGF- and VEGF-receptor related (PVR) and Epidermal Growth
73 Factor Receptor (EGFR), respond to multiple growth factors secreted from the oocyte[20,21].
74 Signaling through PVR/EGFR increases activation of the small GTPase Rac, triggering F-actin
75 polymerization and formation of a major protrusion in the lead border cell[17,19,20,22]. E-Cadherin-
76 based adhesion to the nurse cell substrate stabilizes this lead cell protrusion via a feedback loop
77 with Rac[16]. Furthermore, the endocytic protein Rab11 and the actin-binding protein Moesin
78 mediate communication between border cells to restrict Rac activation to the lead cell[23].
79 Mechanical coupling of border cells through E-Cadherin suppresses protrusions in follower cells,
80 both at cluster exterior surfaces but also between border cells and at contacts with polar cells[13,16].
81 E-Cadherin also maintains border cell attachment to the central polar cells. F-actin and non-

82 muscle myosin II (Myo-II) are enriched at the outer edges of the border cell cluster[24-26]. Such
83 "inside-outside" polarity contributes to the overall cluster shape, cell-cell organization, and
84 coordinated motility of all border cells[13]. While progress has been made in understanding the
85 establishment of front-rear polarity, much less is known about how individual border cell
86 behaviors are fine-tuned and adjusted to produce coordinated and cooperative movement of the
87 cluster as an entire unit.

88 In the current study we made the unexpected discovery that Protein phosphatase 1 (Pp1)
89 activity coordinates the collective behavior of individual border cells. Dynamic cycles of protein
90 phosphorylation and dephosphorylation precisely control many signaling, adhesion and
91 cytoskeletal pathways required for cell migration[27]. Serine-threonine kinases, such as Par-1, Jun
92 kinase (JNK), and the p21-activated kinase Pak3, as well as phosphorylated substrate proteins
93 such as the Myo-II regulatory light chain (MRLC; *Drosophila* Spaghetti squash, Sqh) and
94 Moesin regulate different aspects of border cell migration[15,23,28,29]. In contrast, the serine-
95 threonine phosphatases that counteract these and other kinases and phosphorylation events have
96 not been extensively studied, either in border cells or in other cell collectives. Pp1 is a highly
97 conserved and ubiquitous serine-threonine phosphatase found in all eukaryotic cells[30,31]. Pp1 can
98 directly dephosphorylate substrates *in vitro*, but specificity for phosphorylated substrates *in vivo*
99 is generally conferred by a large number of regulatory subunits (also called Pp1-interacting
100 proteins [PIPs]). These regulatory subunits form functional Pp1 complexes through binding to
101 the Pp1 catalytic (Pp1c) subunits and mediate the recruitment of, or affinity for, particular
102 substrates[31,32]. Thus, despite the potential for pleiotropy, Pp1 complexes have specific and
103 precise cellular functions *in vivo*, that range from regulation of protein synthesis, cell division
104 and apoptosis to individual cell migration[33,34].

We now show that Pp1 activity controls multiple collective behaviors of border cells, including collective polarization, cohesion, cell-cell coordination, and migration. Remarkably, Pp1-inhibited border cells round up, break off from the main group, and move as single cells or small groups but are generally unable to complete their migration. We determine that Pp1 controls the levels of E-Cadherin and β-Catenin, which are needed to retain border cells within a cohesive cluster. Additionally, Pp1 activity restricts F-actin and Myo-II enrichment to the outer edges of the cluster, maintaining a supracellular cytoskeletal ultrastructure and supporting polarized collective movement. Furthermore, the major Pp1 specific complex for Myo-II activity, myosin phosphatase, coordinates border cell shape and adherence of cells to the cluster. Our work thus identifies Pp1 activity, mediated through distinctive phosphatase complexes such as myosin phosphatase, as a critical molecular regulator of collective cell versus single cell behaviors in a developmentally migrating collective.

Results

NiPp1 blocks border cell collective movement and cohesion *in vivo*

To address the role of phosphatases in border cell migration, we carried out a small-scale genetic screen to inhibit selected serine-threonine phosphatases that are expressed during oogenesis using RNAi as well as inhibitors that target catalytic subunits[35]. Inhibition of *Pp4-19C* (one RNAi line) and Pp1c, through overexpression of Nuclear inhibitor of Protein phosphatase 1 (NiPp1), significantly disrupted border cell migration (Supplemental Table 1). NiPp1 is an endogenous protein that when overexpressed, effectively and specifically blocks Pp1 catalytic subunit activity *in vivo*[36-39]. Pp1 and associated complexes are important phosphatase regulators of many cellular processes. Moreover, females expressing NiPp1 driven by *c306*-GAL4 did not produce adult progeny when crossed to wild-type males, consistent with infertility and

suggesting a role for Pp1 in normal oogenesis (Supplemental Figure 1A). Here we focused on further elucidating the function of Pp1 in border cells.

Expression of NiPp1 strongly disrupted both the ability of border cells to organize into a cohesive cluster and to migrate successfully (Figure 1G-J). Unlike control border cells, most NiPp1-expressing border cells failed to reach the oocyte by stage 10 (98%; Figure 1I). Importantly, NiPp1-expressing border cells were no longer found in one cohesive cluster. Instead, individual cells and smaller groups split off from the main cluster (Figure 1H). Whereas control border cells migrated as a single cohesive unit ("1 part"), NiPp1-expressing border cells split into two to three (55%), or more (40%), parts (Figure 1H,J). Migration and cluster cohesion defects were observed when NiPp1 was expressed early in both border cells and the central polar cells (*c306*-GAL4; Figure 1I,J; Supplemental Figure 1B) or later in just border cells (*slbo*-GAL4; Supplemental Figure 1C-G). We observed no defects when NiPp1 was expressed only in polar cells (*upd*-GAL4; Supplemental Figure 1C,H-K). Fragmentation of clusters, however, was stronger when NiPp1 was driven by *c306*-GAL4 rather than *slbo*-GAL4 (compare Figure 1J to Supplemental Figure 1G), possibly due to earlier and higher expression of c306-GAL4 (Supplemental Figure 1B)[40]. Although polar cells are normally located at the center of the border cell cluster and maintain overall cluster organization[16,41], individual NiPp1-expressing border cells could completely separate from polar cells as well as the other border cells (Supplemental Figure 1L-N). Finally, NiPp1 border cells appeared rounder than normal, indicating that individual cell shape regulation was altered (see below). Together, these results demonstrate that NiPp1 expression in border cells, but not polar cells alone, disrupts collective migration, cluster organization and adhesion.

Because very few border cells reached the oocyte, we investigated whether NiPp1-expressing border cells were correctly specified and functional. We first examined the expression of the transcription factor Slbo, the fly C/EBP homolog, which is required for border cell specification in response to JAK/STAT signaling[40,42]. NiPp1-expressing border cells generally expressed Slbo, similarly to control cells (Supplemental Figure 2A-B'; 30/33 border cells expressed Slbo, n = 6 egg chambers). Proper specification through JAK/STAT signaling restricts the number of follicle cells that become migrating border cells[40,43]. When NiPp1 expression was driven by *c306*-GAL4, the total number of cells in the cluster (border cells and polar cells) was slightly increased to a mean of seven NiPp1 cells compared to six control cells per cluster (Supplemental Figure 2C; n = 27 egg chambers for each genotype). This modest increase in cells per cluster is far fewer than what is observed upon ectopic activation of JAK/STAT[40,43], suggesting that NiPp1 does not greatly impact the specification or recruitment of border cells. Thus, NiPp1 prevents properly specified border cells from staying together and completing migration.

Live NiPp1 border cell clusters fall apart and move slowly

To determine where and when NiPp1-expressing border cells stopped migrating and dissociated from the cluster, we examined border cell clusters using live time-lapse imaging[17,44]. Both control and NiPp1 border cells delaminated from the surrounding epithelium and began their migration as a group (Figure 1K-L''; Videos 1-4). NiPp1 border cells separated into multiple sub-collectives or single cells at various points during migration, particularly after moving between the nurse cells (Videos 2-4). NiPp1 border cells typically migrated as small groups but also could arrange themselves into co-linear chains (Video 3). A few NiPp1 border cells reached

the oocyte, although considerably later than control border cells. Indeed, NiPp1-expressing border cells migrated more slowly overall compared to control border cell clusters (~0.35 µm/min NiPp1 versus ~0.65 µm/min control; Figure 1M). Individual NiPp1 border cells also moved at variable speeds, with lagging border cells sometimes pushing ahead of the nominal leading cell (Video 2). Labeling with a cortical cell membrane marker, PLCδ-PH-GFP (*slbo*-GAL4>UAS-PLC δ-PH-GFP), allowed us to determine that some NiPp1 border cells completely disrupted their cell-cell contacts, whereas other border cells remained in contact (Video 5). Finally, single border cells that broke off from the cluster were frequently left behind and stopped moving forward, appearing to get "stuck" between nurse cells (Videos 2-4). Taken together, these data show that NiPp1 disrupts the ability of border cells to maintain a collective mode of migration, and leads to border cells now moving as single cells or small groups with slower speed that typically fail to reach the oocyte.

NiPp1 inhibits the function of Pp1 catalytic subunits in border cells

NiPp1 is a specific inhibitor of Pp1c activity *in vitro* as well as *in vivo*[37-39]. *Drosophila* has four Pp1c subunit genes[45,46], whereas humans have three genes[30]. Pp1α-96A, Flapwing (Flw), and Pp1-87B transcripts are each expressed at moderate-to-high levels in the adult ovary, whereas Pp1-13C RNA is mainly detected in adult males (http://flybase.org/)[47]. We examined the localization of Pp1α-96A using a genomic fosmid transgene in which the open reading frame of Pp1α-96A is driven by its endogenous genomic regulatory regions and C-terminally tagged with GFP ("Pp1α-96A-GFP")[48]. Pp1α-96A-GFP was detected in the cytoplasm, with higher levels at the cortical membranes of border cells, follicle cells, the oocyte, and nurse cells (Figure 2A-C). Endogenous Flw, as visualized using a functional in-frame YFP protein trap[49] ("Flw-YFP"), was

also expressed ubiquitously during the stages in which border cells migrate (Figure 2D-F). Specifically, Flw-YFP was enriched at the cell cortex and cytoplasm of all cells, including border cells. Due to lack of specific reagents, we were unable to determine whether Pp1-87B or Pp1-13C proteins are present in border cells. Therefore, at least two Pp1c subunit proteins are expressed in border cells throughout their migration.

We next determined whether NiPp1 specifically inhibited Pp1c activity in border cells. Overexpression of each of the four *Drosophila* Pp1c subunits individually did not impair border cell migration (Supplemental Figure 3A-E). When co-expressed with NiPp1, two of the catalytic subunits, Pp1α-96A and Pp1-87B, strongly suppressed the migration defects caused by NiPp1, with 90% (NiPp1 + Pp1α-96A) and 80% (NiPp1 + Pp1-87B) of border cells now reaching the oocyte compared to 40% with NiPp1 alone (NiPp1 + RFP; Figure 2G; Supplemental Figure 3F-H). Co-expression of Pp1α-96A and Pp1-87B partially suppressed the NiPp1-induced cluster fragmentation, leading to 55% (NiPp1 + Pp1α-96A) and 65% (NiPp1 + Pp1-87B) of border cell clusters now found intact compared to ~10% with NiPP1 alone (NiPp1 + RFP; Figure 2H; Supplemental Figure 3F-H). Flw and Pp1-13C only mildly suppressed the NiPp1-induced cluster splitting and migration defects (Figure 2G,H; Supplemental Figure 3I,J). The observed phenotypic suppressions were likely due to titration of NiPp1 inhibitory activity by excess Pp1c protein, in agreement with previous studies in *Drosophila*[36,38]. Co-expression of a human Pp1c homolog ("hPPP1CC") fully suppressed the NiPp1-induced phenotypes and did not disrupt migration when expressed on its own (Figure 2G,H; Supplemental Figure 3E,K). hPPP1CC has strong homology to Pp1-87B (93% identical, 96% similar), Pp1α-96A (89% identical, 94% similar), and Pp1-13C (91% identical, 95% similar), although further analysis through the DIOPT (Drosophila RNAi Screening Center Integrative Ortholog Prediction Tool) database

suggests higher homology to Pp1-87B and Pp1α-96A (http://flybase.org/)[50]. The suppression by multiple Pp1 proteins and full suppression by hPPP1CC suggests that Pp1 catalytic subunit genes have overlapping functions in border cells.

To better understand how NiPp1 inhibits Pp1 activity in border cells, we next analyzed the subcellular localization of Flw-YFP and Pp1α-96A-GFP when NiPp1 was co-expressed. Pp1α -96A-GFP and Flw-YFP normally localize to the cortical membrane and cytoplasm of border cells (Figure 2A-F). Upon co-expression with NiPp1, however, Flw-YFP and Pp1α -96A-GFP were now primarily localized to border cell nuclei along with NiPp1 (HA-tagged NiPp1; Supplemental Figure S4A-B"). These results suggest that ectopic NiPp1, in addition to directly inhibiting Pp1c activity[37,38,51], also sequesters PP1 catalytic subunits in the nucleus.

Pp1c genes are required for border cell cluster migration and cohesion

To determine whether Pp1 catalytic activity itself is required for border cell migration, we next downregulated the *Pp1c* genes by driving the respective UAS-RNAi lines in border cells and polar cells with *c306*-GAL4 (Figure 3A-D). RNAi lines that target 3 of the 4 catalytic subunits (Pp1α-96A, Pp1-87B, and Pp1-13C) strongly disrupted border cell migration (Figure 3B-E). Knockdown of *Pp1c* genes also caused ≥ 50% of border cell clusters to dissociate into multiple sub-clusters and single cells (Figure 3B-D,F). Using live imaging, we confirmed that decreased levels of Pp1α-96A, Pp1-87B, and Pp1-13C by RNAi altered border cell migration and caused cells to split from the main cluster (Figure 3G; Videos 6-9). Multiple *flw* RNAi lines (see Materials and Methods) did not impair migration or cluster cohesion when expressed in border cell clusters. However, RNAi does not always fully knock down gene function in cells[52]. As complete loss of *flw* is homozygous lethal, we generated border cells that were mosaic mutant for

the strong loss of function allele *flw*^{FP41} [ref 53]. Mosaic *flw*^{FP41} border cell clusters were typically composed of a mixture of wild-type and mutant cells and frequently fell apart, with ~90% splitting into two or more parts (Figure 3H-I; Supplemental Figure 4C-C"). In egg chambers with *flw* mutant border cells, 40% of border cells did not migrate at all whereas 20% of border cells partially migrated but did not reach the oocyte (Figure 3H-H",J; Supplemental Figure 4C-C"). NiPp1 expression results in more severe phenotypes than RNAi knockdown, or loss, of individual *Pp1c* genes, suggesting that Pp1c subunits have distinct and overlapping functions in border cell cohesion and migration.

Pp1 promotes cadherin-catenin complex levels and adhesion of border cells

One of the strongest effects of decreased Pp1c activity was the dissociation of border cells from the cluster. In many cell collectives, cadherins critically mediate the attachment of individual cells to each other during migration, although other cell-cell adhesion proteins can also contribute[9,54]. The cadherin-catenin complex members E-Cadherin (*Drosophila* Shotgun; Shg), β-Catenin (*Drosophila* Armadillo; Arm) and α-Catenin are all required for border cell migration[16,41,55-57]. E-Cadherin, in particular, is required for traction of border cells upon the nurse cell substrate, for producing overall front-rear polarity within the cluster, and for attachment of border cells to the central polar cells[16,41]. Complete loss of cadherin-catenin complex members in border cells prevents any movement between nurse cells[41,55,56]. This has precluded a definitive analysis of whether all, or some, complex members promote adherence of border cells to the polar cells and/or to other border cells.

To determine whether adhesion of border cells to the cluster requires a functional cadherin-catenin complex, we used *c306*-GAL4 to drive RNAi for each gene in all cells of the

cluster (polar cells and border cells; Supplemental Figure 1B). Multiple non-overlapping RNAi lines for E-Cadherin, β-Catenin, and α-Catenin each reduced the respective endogenous protein levels and disrupted border cell migration, in agreement with previous results that used mutant alleles (Figure 4A-E,G,I; Supplemental Figure 5A-F')[41,55,57]. Importantly, RNAi knockdown for each of the cadherin-catenin complex genes, driven in both polar cells and border cells, resulted in significant fragmentation of the border cell cluster compared to controls. E-Cadherin (40-50%) and β-Catenin (55-80%) RNAi lines exhibiting stronger, while α-Catenin RNAi lines exhibited milder (~20-30%), cluster fragmentation (Figure 4A-D,F,H,J; Video 10). Dissociated RNAi border cells could localize to the side of the egg chamber (Figure 4B,D), although others remained on the normal central migration pathway (Figure 4C,D). While α-Catenin RNAi knockdown in polar cells alone (*upd*-GAL4) caused border cell cluster splitting and migration defects, this effect was significantly milder than the effects of α-Catenin knockdown in both polar cells and border cells (compare Figure 4I,J to Supplemental Figure 5G,H). These results indicate that the cadherin-catenin complex keeps border cells attached to each other and to the polar cells, which in turn maintains a cohesive cluster.

We next wanted to determine whether Pp1 regulated these adhesion proteins in border cells. We analyzed the levels and localization of E-Cadherin and β-Catenin at cell-cell contacts in NiPp1-expressing border cell clusters that were still intact or loosely connected (Figure 4K-P). In wild-type clusters, E-Cadherin and β-Catenin are highly enriched at cell contacts between border cells (BC-BC) and between border cells and polar cells (BC-PC; Figure 4K-K",M-M"). NiPp1-expressing border cell clusters exhibited reduced levels of E-Cadherin and β-Catenin at most BC-BC contacts (Figure 4L-L",N-N"). Pp1-inhibited polar cells generally retained E-Cadherin and β-Catenin, which was higher compared to border cells (Figure 4L-L",N-N"). We

quantified the relative levels of E-Cadherin (Figure 4O) and β-Catenin (Figure 4P) at BC-BC contacts in control versus NiPp1 clusters, normalized to the levels of those proteins at nurse cell-nurse cell junctions. Both E-Cadherin and β-Catenin were reduced by almost half compared to matched controls. These data together suggest that Pp1 activity regulates cadherin-catenin proteins at cell-cell contacts, which contributes to adhesion of border cells within the cluster.

Pp1 activity promotes protrusion dynamics but is dispensable for directional migration

Border cells with impaired Pp1 activity migrated significantly slower than control clusters (Figures 1M, 3G), suggesting that border cell motility was altered. Migrating cells form actin-rich protrusions at the front, or leading edge, which help anchor cells to the migratory substrate and provide traction for forward movement[58,59]. In collectives, protrusive leader cells also help sense the environment to facilitate directional migration[8]. Border cells typically form one or two major protrusions at the cluster front[17,19,22] (Figure 5A-A"",C; Supplemental Figure 6A; Video 6). Pp1-inhibited border cells (Pp1c RNAi) still extended forward-directed protrusions (Figure 5A-C; Videos 7-9). Additionally, the numbers, lifetimes, lengths and areas of side- and back-directed protrusions were not generally increased in Pp1-inhibited border cell clusters compared to control (Figure 5C-F; Supplemental Figure 6B,C). However, the number of protrusions produced at the front of the cluster was reduced in Pp1 RNAi border cells (range of 0.5-0.85 mean protrusions per frame, all genotypes) compared to control (1.0 mean protrusions per frame; Figure 5C). Additionally, the lifetimes of Pp1 RNAi forward-directed protrusions were reduced (Figure 5D). Control protrusions at the cluster front had a lifetime of ~18 min, whereas Pp1-inhibited front protrusions persisted for 5-10 min. These short-lived Pp1 RNAi protrusions were also reduced in length, from a third to half the size of control front-directed protrusions (Figure

5E; Supplemental Figure 6B). Further, Pp1-inhibited front protrusions were smaller, with a mean area of ~10-20μm^2 compared to the control mean of ~40μm^2 (Figure 5F; Supplemental Figure 6C). Thus, Pp1 activity promotes normal protrusion dynamics, including the number, lifetime and size of front-directed protrusions.

NiPp1 and Pp1c RNAi border cells followed the normal migratory pathway down the center of the egg chamber between nurse cells, even when cells broke off from the main cluster (Figures 1H, L-L" and 3B-D; Videos 2-5, 7-9). Moreover, in Pp1 RNAi border cells, front-directed protrusions still formed though with altered dynamics. These observations together suggest that Pp1 activity is not required for directional migration. To further test this idea, we made use of a Förster Resonance Energy Transfer (FRET) activity reporter for the small GTPase Rac. Normally, high Rac-FRET activity occurs at the cluster front during early migration in response to guidance signals from the oocyte, and correlates with protrusion extension (Supplemental Figure 6D)[22]. Under conditions of PP1-inhibition, the most severely affected clusters fall apart, sometimes on different focal planes. This potentially complicates interpretation of Rac-FRET signals. We therefore measured Rac-FRET only in those NiPp1-expressing border cell clusters that remained intact. We detected elevated Rac-FRET activity in NiPp1 border cells similar to control, indicating that Rac activity was largely preserved although with slightly elevated levels (Supplemental Figure 6D,E). In sum, these data indicate that Pp1 activity influences protrusion dynamics and cell motility, but does not appear to be critical for directional orientation of the cluster to the oocyte.

Pp1 promotes border cell shape through collectively polarized F-actin and Myo-II

Migrating cells, including cell collectives, change shape to facilitate their movement through complex tissue environments[60]. Some cells maintain a single morphology, such as an elongated mesenchymal or rounded amoeboid shape, throughout migration, whereas other cells interconvert from one shape to another as they migrate. The border cell cluster overall is rounded, although individual border cells within the group appear slightly elongated (Figure 6A,A'; Videos 1 and 6)[24]. However, NiPp1 border cells, whether present in small groups or as single cells, were visibly rounder than control border cells (Figure 1H,L-L"; Videos 1-4). We observed similar cell rounding when the *Pp1c* genes were knocked down by RNAi, although some border cells appeared more noticeably round than others (Figures 3B-D, 5B-B""; Videos 7-9). To quantify these altered cell shapes, we expressed the membrane marker PLC δ-PH-GFP to visualize individual cells within the cluster and measured "circularity", which indicates how well a shape approaches that of a perfect circle (1.0; Figure 6A-C). Control border cells overall were slightly elongated with a mean of ~0.7, although the circularity of individual cells varied substantially (range of ~0.4 to 0.95), suggesting that border cells undergo dynamic shape changes during migration (Figure 6C). In contrast, NiPp1 border cells were rounder, with a mean of ~0.9, and exhibited less variation than control (range of ~0.7 to 1.0; Figure 6C).

The rounder cell shapes suggested that Pp1 inhibition alters the cortical cytoskeleton of the border cells. Wild-type border cells exhibit a marked enrichment of F-actin at the cluster periphery, whereas lower levels are detected inside the cluster at contacts between border cells (Figure 6D,D',F; Video 11)[25,61]. Upon Pp1 inhibition, F-actin now accumulated around each individual border cell, especially at BC-BC membrane contacts, rather than just being enriched at outer cluster surfaces (Figure 6E,E',G; Video 12). Similarly, Myo-II as visualized by GFP-tagged Spaghetti Squash (Sqh-GFP), the *Drosophila* homolog of the myosin regulatory light

chain (MRLC), is highly dynamic and normally concentrates at the outer periphery of live border cell clusters both during early (Figure 6H-H””’; Video 13) and later stages of migration (Supplemental Figure 7A-A””’; Video 15)[24,26,28]. In NiPp1 border cells, however, Sqh-GFP accumulated more uniformly at the cortical membranes of each border cell especially during early migration (Figure 6I-I””’; Video 14), but also at later stages (Supplemental Figure 7B-B””’; Video 16). Thus, inhibition of Pp1 converts collectively polarized F-actin and Myo-II to that characteristic of single migrating cells. As a result, individual border cells now have enriched actomyosin localization consistent with elevated cortical contractility at the single cell level.

Pp1 promotes actomyosin contractility in border cells through myosin phosphatase

Rok and other kinases phosphorylate the Myo-II regulatory light chain Sqh[62]. This leads to fully activated Myo-II, which then forms bipolar filaments, binds to F-actin, and promotes cell contractility. Given the altered distribution of Sqh-GFP when Pp1 was inhibited, we next analyzed the levels and distribution of active Myo-II. We used an antibody that recognizes phosphorylated Sqh at the conserved Ser-21 (mammalian MRLC Ser-19)[28]. Control border cells exhibit p-Sqh signal at the cluster periphery (Figure 7A, A’), closely resembling the pattern of Sqh-GFP in live wild-type border cells (Figure 6H-H””’)[24,28]. NiPp1 border cells, however, had high levels of p-Sqh distributed throughout the cluster including at internal BC-BC contacts (Figure 7B,B’), similar to Sqh-GFP in live NiPp1 border cells (Figure 6I-I””’). These data support the idea that Pp1 inhibition elevates myosin activation.

Myo-II undergoes cycles of activation and inactivation via phosphorylation and dephosphorylation, respectively, to generate dynamic cellular contraction *in vivo*[62]. We

380 previously showed that waves of dynamic Myo-II maintain the collective morphology of border
381 cells to facilitate movement through the egg chamber[24]. The myosin phosphatase complex
382 consists of a Pp1c subunit and a specific regulatory subunit, the myosin binding subunit (Mbs;
383 also called myosin phosphatase-targeting subunit [MYPT]), which together dephosphorylate Sqh
384 and inactivate Myo-II[63]. Previously, we found that Mbs was required for border cell cluster
385 delamination from the epithelium and cell shape[24,28]. We therefore wanted to determine whether
386 myosin phosphatase contributed to the above-described Pp1 functions in cell shape, cluster
387 cohesion and migration. First, we confirmed that Mbs transcript and protein were expressed in
388 border cells throughout migration (Supplemental Figure 8A-F). Mbs protein colocalized with
389 Pp1c subunits near border cell membranes and in the cytoplasm (Supplemental Figure 8G-I"). In
390 general, Mbs colocalized more extensively with Flw-YFP than with Pp1α-96A-GFP
391 (Supplemental Figure 8G-J). Next, we analyzed the functions of Mbs in border cells using an
392 RNAi line that specifically reduced endogenous levels of Mbs (Supplemental Figure 8K-L").
393 Border cells deficient for Mbs were rounder than control border cells, exhibited incomplete
394 migration (~30%), and separated from the cluster (60%) along the migration pathway (Figure
395 7C-F). These findings indicate that myosin phosphatase, a specific Pp1 complex, promotes the
396 normal cell morphology and collective cohesion of border cells, in addition to helping border
397 cells migrate successfully to the oocyte.

398 RhoA activates Rho-associated kinase (Rok), thus leading to activation of Myo-II[62]. We
399 and others previously found that expression of constitutively-activated RhoA (*Drosophila* Rho1)
400 causes markedly rounder border cells and alters the distribution of F-actin and Myo-II at cell-cell
401 contacts between border cells[24,26]. We therefore investigated whether Pp1 regulated RhoA
402 activity in migrating border cells. We used a FRET construct that was recently shown to

403 specifically report RhoA activity in ovarian follicle cells[64]. Inhibition of Pp1 by NiPp1
404 moderately increased the overall levels of Rho-FRET in intact border cell clusters compared to
405 control border cells (Supplemental Figure 9A-C). These data suggest a general upregulation of
406 the RhoA pathway upon Pp1 inhibition.

407
408 **Discussion**

409 To migrate collectively, cells need to coordinate and cooperate at the multicellular level.
410 Individual cells within a group must remain together, maintain optimal cell shapes, organize
411 motility of neighboring cells, and polarize. The mechanisms that globally orchestrate single cell
412 behaviors within migrating cell collectives are still unclear. Here we report that Pp1 activity is a
413 critical regulator of key intra- and intercellular mechanisms that together produce collective
414 border cell migration. Loss of Pp1 activity, through overexpression of NiPp1 or Pp1c RNAi,
415 switches border cells from migrating as a cohesive cluster to moving as single cells or in small
416 groups (Figure 8A). A critical aspect of this switch is the redistribution of enriched F-actin and
417 Myo-II to cell contacts between individual border cells, rather than at the cluster periphery, and a
418 concomitant loss of adhesion between cells. We identified one key Pp1 phosphatase complex,
419 myosin phosphatase, that controls collective-level myosin contraction (Figure 8B). Additional
420 phosphatase complexes, through as-yet-unknown regulatory subunits, likely function in border
421 cells to generate collective F-actin organization, maintain cell-cell adhesions, and potentially to
422 restrain overall RhoA activity levels. Our results support a model in which balanced Pp1 activity
423 promotes collective border cell cluster migration by coordinating single border cell motility and
424 keeping the cells together (Figure 8A).

425 Many collectively migrating cells require a supracellular enrichment of actomyosin at the
426 group perimeter to help organize their movement[7,10-12]. Active Myo-II is required for border cell

collective detachment from the epithelium, cluster shape, rotational movement of the cluster, and normal protrusion dynamics[24,26,28,65]. We show here that Pp1 organizes collective-level Myo-II-contractility during border cell migration. Inhibition of Pp1 shifts the balance of activated Myo-II from the cluster-level to individual border cells, resulting in rounded, hyper-contractile border cells that dissociate from the cluster. The myosin-specific Pp1 complex, myosin phosphatase, directly dephosphorylates Sqh and inhibits Myo-II activation[63]. Depletion of Mbs, the myosin-binding regulatory subunit of myosin phosphatase, causes rounder border cells and fragmentation of the cluster. We previously found that Mbs-deficient border cells have significantly higher levels of phosphorylated Sqh[28]. Thus, myosin phosphatase inhibits Myo-II activation to promote coordinated collective contractility of border cells. Myosin phosphatase is a downstream target of Rok, which phosphorylates and inhibits the Mbs subunit[66]. Consistent with loss of myosin phosphatase activity, Pp1-inhibition increases phosphorylated active Sqh at internal border cell junctions within the cluster. Thus, myosin phosphatase, downstream of Rok, promotes elevated active Myo-II and cortical contraction of the entire collective (Figure 8B). Interestingly, expression of constitutively activated RhoA also induces cellular hypercontractility, resulting in amoeboid-like round border cells[24,26]. RhoA activates Rok, which directly phosphorylates and activates the Myo-II regulatory subunit Sqh[67,68]. We observed somewhat elevated RhoA activity in the absence of Pp1 activity. Thus, Pp1 may also restrain the overall levels of RhoA activity in border cells through an unknown Pp1 complex, which would further promote the collective actomyosin contraction of border cells (Figure 8B).

Myo-II is activated preferentially at the cluster periphery and not between internal border cell contacts. Mbs and at least one catalytic subunit, Flw, localize uniformly in border cells, both on the cluster perimeter and between cells. Such uniform phosphatase distribution would be

450 expected to dephosphorylate and inactivate Myo-II everywhere, yet phosphorylated Sqh is only
451 absent from internal cluster border cell contacts. Rok phosphorylates and inactivates Mbs in
452 addition to directly activating Myo-II[66]. Our previous results indicate that Rok localizes to the
453 cluster perimeter similar to p-Sqh, but there appeared to be overall less Rok between border
454 cells[24]. Thus, spatially localized Rok could inhibit myosin phosphatase and activate Myo-II
455 preferentially at the outer edges of the cluster (Figure 8A). Other mechanisms likely contribute to
456 collective polarization of Myo-II. For example, during border cell detachment from the
457 epithelium the polarity kinase Par-1 phosphorylates and inactivates Mbs at the cluster rear
458 resulting in increased active Myo-II, whereas the Hippo pathway prevents accumulation of
459 phosphorylated Myo-II between border cells[25,28].

460 Our data also support a role for Pp1 in controlling F-actin stability, dynamics, and spatial
461 organization. Similar to the pattern of activated Myo-II, cortical F-actin is normally high at the
462 cluster periphery, although low levels are found between border cells[23,25,61]. Reduced Pp1
463 activity causes high levels of F-actin to redistribute from the cluster perimeter to surround entire
464 cell cortices of individual border cells. In migrating cells, networks of F-actin produce forces
465 essential for protrusion extension and retraction dynamics that generate forward movement[58,59].
466 Further supporting a role for Pp1 in regulating F-actin, Pp1-inhibited border cells extend fewer
467 protrusions with shorter lifetimes, resulting in altered motility patterns. How Pp1 promotes F-
468 actin organization and dynamics is unknown. One possibility comes from the known function for
469 Rok in regulating F-actin through the downstream effector LIM Kinase (LIMK)[69]. LIMK
470 phosphorylates and inhibits cofilin, an actin severing and depolymerizing factor[70]. In border
471 cells, cofilin restrains F-actin levels throughout the cluster and increases actin dynamics,
472 resulting in normal cluster morphology and major protrusion formation[71]. Although cofilin

473 dephosphorylation, and thus activation, is typically mediated by the dual-specificity phosphatase
474 Slingshot[70], Pp1-containing complexes have been shown to dephosphorylate cofilin in a variety
475 of cell types[72-75]. Additionally, RhoA activates formin proteins such as Diaphanous, which
476 nucleate actin to form long filaments[76]. There are at least seven formin-related proteins in
477 *Drosophila*, several of which have domains associated with activation by Rho GTPases.
478 However, which formin, if any, promotes border cell migration and F-actin distribution is
479 unknown. Further work will be needed to determine whether any of these potential targets, or
480 other actin regulatory proteins, control collective level F-actin enrichment via Pp1.

481 A major consequence of decreased Pp1 activity is fragmentation of the border cell cluster
482 into single border cells and small groups. This raises the question of how Pp1 activity maintains
483 cluster cohesion, which is critical for collective cell movement *in vivo*. Like many cell
484 collectives, high levels of cadherin-catenin complex proteins are detected between all border
485 cells[9,41]. We found that Pp1 maintains E-Cadherin and β-Catenin levels between border cells.
486 Thus, cluster fragmentation upon Pp1 inhibition could at least partly be due to deficient
487 cadherin-catenin adhesion. The cadherin-catenin complex is required for border cells to adhere to
488 the central polar cells as well as to provide migratory traction of the entire cluster upon the nurse
489 cells[16,41]. Our results indicate that E-Cadherin, β-Catenin, and α-Catenin maintain adhesion of
490 border cells to each other in addition to the polar cells. Knockdown of the cadherin-catenin
491 complex members in both border cells and polar cells causes border cells to significantly
492 dissociate from the cluster. The requirement for cadherin-catenin in cluster cohesion may have
493 been masked in prior studies due to the inability of loss-of-function cadherin-catenin mutant
494 border cells to move at all[16,41,55,56]. While RNAi for E-Cadherin, β-Catenin, and α-Catenin each
495 strongly knock down the respective protein levels, it may be that a small amount of each protein

is still present. Such remaining cadherin-catenin proteins may provide just enough traction for border cells to partially migrate upon the nurse cells. We speculate that movement of cadherin-catenin-deficient border cells within the confining tissue would provide mechanical stresses that break the cluster apart at weakened border cell-border cell contacts. Indeed, a mutant α-Catenin protein that lacks part of the C-terminal F-actin-binding domain was shown to partially rescue the migration defects caused by loss of *α-Catenin*; however, these rescued border cell clusters split into several parts along the migration path[56]. Further supporting this idea, Pp1-inhibited border cells fall apart during their effort to migrate between the nurse cells.

How does Pp1 promote cluster cohesion? Given the effects of Pp1 on E-Cadherin and β-Catenin at internal border cell contacts, and the requirement for cadherin-catenin complex proteins in maintaining cluster integrity, Pp1 could directly regulate cadherin-catenin protein stability and/or adhesive strength. In mammalian and *Drosophila* cells, phosphorylation of a conserved stretch of serine residues in the E-Cadherin C-terminal tail region regulates E-Cadherin protein stability, binding of E-Cadherin to β-Catenin, and cell-cell junction formation and turnover[77-79]. Serine-phosphorylation of α-Catenin is also required for adhesion between epithelial cells and may be required for efficient border cell migration[80]. More work will be needed to determine whether a to-be-identified Pp1-containing phosphatase complex directly dephosphorylates E-Cadherin and/or α-Catenin, as the roles for phosphatases in cadherin-catenin junctional stability are still poorly understood. Alternatively, or in addition, Pp1 regulation of collective actomyosin contraction at the cluster periphery could allow internal cluster cell-cell junctions to be maintained. Pp1-inhibition greatly alters actomyosin distribution, causing individual border cells to contract and round up. The forces transmitted by high cell contractility alone could weaken adherens junctions, causing the border cells to break apart during migration

519 (Figure 8A). Myosin phosphatase-depleted border cells, which have elevated phosphorylated
520 Sqh[28] and thus active Myo-II, are highly contractile, round up, and fall off the cluster. Thus,
521 collective-level active actomyosin contraction contributes to keeping border cells adhered to the
522 cluster. Of note, Myo-II and cadherin-catenin complexes have dynamic and quite complex
523 interactions that influence stability of cell-cell junctions, and which may depend on cellular
524 context[81,82]. NiPp1 expression disrupts cluster cohesion to a greater extent than knockdown of
525 either myosin phosphatase or cadherin-catenin complex members alone. This suggests that
526 cadherin-catenin phosphorylation and optimal actomyosin activity both contribute to cluster
527 cohesion through distinct Pp1 phosphatase complexes, although this possibility remains to be
528 formally tested (Figure 8B).

529 Our study implicates Pp1 as a key regulator of collective cohesion and migration in
530 border cells. Pp1 catalytic subunits and their regulatory subunits are conserved across
531 eukaryotes[30-32,34]. The roles of specific Pp1 complexes in collective cell migration during
532 development and in cancer have not been well studied. Intriguingly, Mypt1 (Mbs homolog)
533 promotes polarized mesodermal migration during zebrafish gastrulation[83]. Similar to what we
534 observe in Mbs-depleted border cells, inhibition of zebrafish Mypt1 switched cells from an
535 elongated mesenchymal mode of migration to a hyper-contractile amoeboid mode of migration.
536 Another Pp1 phosphatase complex containing the Phactr4 (phosphatase and actin regulator 4)
537 regulatory subunit promotes the chain-like collective migration of enteric neural crest cells,
538 which colonize the gut and form the enteric nervous system during development[74]. Phactr4,
539 through Pp1, specifically controls the directed migration and shape of enteric neural crest cells
540 through integrin, Rok, and cofilin. Given the conservation of these and other phosphatase

complexes, our study highlights the importance of balanced Pp1 phosphatase activity in the organization and coordination of migrating cell collectives.

Materials and Methods

Drosophila genetics and strains

Crosses were generally set up at 25°C unless otherwise indicated. The *tub*-GAL80^{ts} ("tsGAL80") transgene[84] was included in many crosses to suppress GAL4-UAS expression during earlier stages of development; these crosses were set up at 18˚-22˚C to turn on tsGAL80. For *c306*-GAL4, *c306*-GAL4-tsGal80, *slbo*-GAL4, or *upd*-GAL4 tsGAL80 crosses, flies were incubated at 29°C for ≥ 14 h prior to dissection to produce optimal GAL4-UAS transgene expression. *c306*-GAL4 is expressed early and more broadly in border cells, polar cells, and terminal (anterior and posterior) follicle cells (Supplemental Figure 1B)[40]. During oogenesis, *slbo*-GAL4 turns on later than *c306*-GAL4, and is expressed in border cells but not polar cells, as well as a few anterior and posterior follicle cells at stage 9 (Supplemental Figure 1C,D)[40,85]. *upd*-GAL4 is restricted to polar cells at all stages of oogenesis (Supplemental Figure 1C,H)[16]. Mosaic mutant clones of *flw* were generated using the FLP-FRT system[86]. The *flw*^{FP41} FRT 19A line was crossed to *ubi*-mRFP.nls *hs*FLP FRT19A; the resulting progeny were heat shocked for 1 h at 37°C, two times a day for 3 d, followed by 3 d at 25°C prior to fattening and dissection. Mutant clones were identified by loss of nuclear RFP signal from *ubi*-mRFP.nls.

The following *Drosophila* strains (with indicated stock numbers) were obtained from the Bloomington Drosophila Stock Center (BDSC, Bloomington, IN, USA): *c306*-GAL4 (3743), UAS-NiPp1.HA (23711), UAS-Pp1-87B.HA (24098), UAS-Pp1-13C.HA (23701), UAS-Pp1α-96A.HA (23700), UAS-hPPP1CC (64394), UAS-mCD8.ChRFP (27392), UAS-mCherry RNAi

564 (35785), UAS-Pp2B-14D RNAi (25929, 40872), UAS-mts RNAi (27723, 38337, 57034, 60342),
565 UAS-Pp4-19C RNAi (27726, 38372, 57823), UAS-CanA-14F RNAi (38966), UAS-PpD3 RNAi
566 (57307), UAS-PpV RNAi (57765), UAS-CanA1 RNAi (25850), UAS-CG11597 RNAi (57047,
567 61988), UAS-rgdC RNAi (60076), UAS-Flw RNAi (38336), UAS-β-Catenin RNAi JF01252
568 (31305), *flw*^{FP41} FRT 19A (51338), ubi-mRFP.nls hsFLP FRT19A (31418), UAS-PLCδ-PH-GFP
569 ("membrane GFP"; 39693).

570 The following *Drosophila* strains (with indicated stock numbers) were obtained from the
571 Vienna Drosophila Resource Center (VDRC, Vienna, Austria): UAS-Pp1α-96A RNAi (v27673),
572 UAS-Pp1-87B RNAi (v35024), UAS-Pp1-13C RNAi (v29058), UAS-Flw RNAi (v29622,
573 v104677), UAS-Mbs RNAi (v105762), UAS-Pp2B-14D RNAi (v46873), UAS-Pp4-19c RNAi
574 (25317), UAS-E-Cadherin RNAi (v27082, v103962), UAS-β-Catenin RNAi (v107344), UAS-α-
575 Catenin RNAi (v20123, v107298), fTRG Pp1α -96A (v318084), fTRG Sqh (v318484),.

576 Other *Drosophila* strains used in this study were: *slbo*-GAL4, *slbo*-GAL4 UAS-
577 mCD8::GFP, *upd*-GAL4;; tsGAL80, and *slbo*-LifeAct-GFP line 2M (from D. Montell,
578 University of California, Santa Barbara, Santa Barbara, CA, USA), *flw*^{CPTI002264} protein trap (line
579 115284, Kyoto Stock Center, Kyoto, Japan), UAS-mCherry-Jupiter (from C. Doe, University of
580 Oregon, Eugene, OR, USA), UAS-Rac FRET[22], UAS-Rho FRET/CyO; UAS-Rho
581 FRET/TM6B[64], and UAS-Flw.HA (FlyORF)[87]. The *c306*-GAL4 tsGAL80[24] and *c306*-GAL4
582 tsGAL80/FM6; UAS-NiPp1.HA/TM3 Ser stocks were created in our lab.
583

584 **Female fertility test**

585 Fertility was determined according to established methods[88]. Briefly, four *c306*-GAL4
586 tsGAL80/FM6; Sco/CyO (control) or *c306*-GAL4 tsGAL80/FM6; UAS-NiPP1/TM3 Ser

(experimental) females were outcrossed to four w^{1118} males. The flies were allowed to mate for 2 days followed by a 24 h egg lay at 30˚C on fresh food medium supplemented with yeast. Adults were then removed and the progeny allowed to develop in the vial at 25˚C; the food was periodically monitored to avoid drying out. Scoring of eclosed adult progeny from each vial was performed 16-20 d after egg laying and reported as the average progeny per female.

Immunostaining

Fly ovaries from 3- to 5-d-old females were dissected in Schneider's Drosophila Medium (Thermo Fisher Scientific, Waltham, MA, USA) supplemented with 10% fetal bovine serum (Seradigm FBS; VWR, Radnor, PA, USA). Ovaries were kept whole or dissected into individual egg chambers, followed by fixation for 10 min using 4% methanol-free formaldehyde (Polysciences, Warrington, PA, USA) in 0.1 M potassium phosphate buffer, pH 7.4, or in 1X Phosphate Buffered Saline (PBS). Washes and antibody incubations were performed in "NP40 block" (50 mM Tris-HCl, pH 7.4, 150 mM NaCl, 0.5% NP40, 5 mg/ml bovine serum albumin [BSA]). For α-Catenin immunostaining, dissected egg chambers were fixed for 20 min in 4% paraformaldehyde (Electron Microscopy Sciences, Hatfield, PA, USA) in potassium phosphate buffer, pH 7.4, followed by a separate blocking step for 30 min (2% BSA in 1x PBS) prior to each antibody incubation. For p-Sqh antibody staining, dissected stage 11 and older egg chambers were manually discarded to ensure that the signal in earlier stages was not diluted; overnight primary incubation at 4˚C was performed with rocking. For the F-actin staining in Figure 6, the entire dissection procedure was performed in less than 10 min to preserve F-actin structures, followed by fixation in the presence of Phalloidin at 1:400 dilution; after washing off the fix, the egg chambers were incubated in Phalloidin at 1:400 for 2 h[89].

610 The following primary antibodies from the Developmental Studies Hybridoma Bank
611 (DSHB, University of Iowa, Iowa City, IA, USA) were used at the indicated concentrations: rat
612 anti-E-Cadherin 1:10 (DCAD2), mouse anti-Fasciclin III 1:10 (FasIII; 7G10), mouse anti-Arm
613 (β-Catenin) 1:75 (N2-7A1), concentrated rat anti-α-Catenin 1:1000 (DCAT1), mouse anti-Eyes
614 Absent 1:100 (eya10H6), mouse anti-Lamin Dm0 1:10 (ADL67.10), and mouse anti-Singed 1:25
615 (Sn7C). Additional primary antibodies used were: rabbit anti-Phospho-Myosin Light Chain 2
616 (Ser19) 1:40 (#3671, Cell Science Technology, Danvers, MA, USA), rat anti-HA 1:1000
617 (11867423001, Millipore Sigma, Burlington, MA, USA), rabbit anti-Mbs 1:200 (from C. Tan,
618 University of Missouri, Columbia, MO, USA); rabbit anti-GFP polyclonal 1:1000-1:2000 (A-
619 11122, Thermo Fisher Scientific), chicken anti-GFP polyclonal 1:1000 (ab13970, Abcam,
620 Cambridge, MA, USA), rat anti-Slbo 1:2000 (from P. Rørth, Institute of Molecular and Cell
621 Biology, Singapore). Alexa Fluor 488, 568, or 647 secondary antibodies (Thermo Fisher
622 Scientific) were used at 1:400 dilution. Alexa Fluor Phalloidin (488 or 568; Thermo Fisher
623 Scientific) and Phalloidin–Atto 647N (Millipore Sigma) were used at 1:400 dilution. 4',6-
624 Diamidino-2-phenylindole (DAPI, Millipore Sigma) was used at 0.05 µg/ml. Egg chambers were
625 mounted on slides with Aqua-Poly/Mount (Polysciences) or FluorSave Reagent (Millipore
626 Sigma) for imaging.
627
628 **Microscopy, live time-lapse imaging, and FRET**
629 Images of fixed egg chambers were acquired with an upright Zeiss AxioImager Z1 microscope
630 and Apotome.2 optical sectioning, or on a Zeiss LSM 880 confocal microscope (KSU College of
631 Veterinary Medicine Confocal Core), using either a 20× 0.75 numerical aperture (NA) or 40× 1.3
632 NA oil-immersion objective.

Live time-lapse imaging was performed as described[17,44]. Briefly, ovarioles were dissected in room-temperature sterile live imaging media (Schneider's Drosophila Medium, pH 6.95, with 15–20% FBS). Fresh live imaging media, supplemented with 0.2 µg/ml bovine insulin (Cell Applications, San Diego, CA, USA), was added to the sample prior to mounting on a lumox® dish 50 (94.6077.410; Sarstedt, Newton, NC, USA). Time-lapse videos were generally acquired at intervals of 2–3 min for 3-6 h using a 20× Plan-Apochromat 0.75 NA objective, a Zeiss Colibri LED light source, and a Zeiss Axiocam 503 mono camera. The LED light intensity was experimentally adjusted to maximize fluorescence signal and to minimize phototoxicity of the live sample. Live time-lapse Sqh-GFP imaging was performed on a Zeiss LSM 880 confocal, as described[44], with a 40× 1.2 NA water-immersion objective using an interval of 1 min for up to 10 min total time and a laser setting of 5%. In some cases, multiple *z*-stacks were acquired and merged in Zeiss AxioVision, Zeiss ZEN 2, or FIJI[90] to produce a single, in-focus time-lapse video.

FRET images (Rac FRET, Rho FRET) of live cultured egg chambers were acquired with a Zeiss LSM710 microscope essentially as described[22]. A 40× 1.3 NA oil inverted objective was used to capture single high-resolution stationary images. A 458 nm laser was used to excite the sample. CFP and YFP emission signals were collected through channel I (470–510 nm) and channel II (525–600 nm), respectively. The CFP and YFP channels were acquired simultaneously for most experiments. Sequential acquisition of CFP and YFP channels was tested but produced the same result as simultaneous acquisition.

Image processing and data analysis

Image measurements and editing were performed using Zeiss ZEN 2 or FIJI[90]. Analyses of live border cell migration time-lapse videos was performed using Zeiss ZEN 2 software. The migration speed was calculated from the duration of border cell movement. Protrusion quantification was performed as described[91]. Briefly, a circle was drawn around the cell cluster, and extensions greater than 1.5 μm outside the circle were defined as protrusions (Supplemental Figure 6A). Protrusions were classified as directed to the front (0°-45° and 0°-315°), side (45°-135°and 225°-315°), or back (135°-225°), based on their positions within the cluster. The first 1 h of each video was used for protrusion quantification.

To determine the number of cells per cluster, egg chambers were stained for the nuclear envelope marker Lamin, the DNA stain DAPI, and the cell membrane marker E-Cadherin. Only clusters that had delaminated, moved forward, and had any detectable E-Cadherin were imaged. This allowed confidence that the scored cells were border cells. Acquisition of *z*-stacks that encompassed the entire cluster (border cells and polar cells) were defined by nuclear Lamin signal. This was followed by manual counting of the nuclei from the resulting images.

The circularity of border cells was measured in FIJI. Individual border cells were outlined manually based on the PLCδ-PH-GFP signal using the "Freehand Selections" tool. Within the "Set Measurements" analysis tool, "shape descriptors" was selected, followed by the "Measure" function, which provided a measurement of circularity. A value of 1.0 indicates a perfect circle, whereas 0.0 represents an extremely elongated shape.

Measurements of E-Cadherin and β-Catenin intensity at cell–cell junctions were performed on egg chambers that were stained using identical conditions. Samples were imaged with a 40× 1.3 NA oil objective. Identical confocal laser settings were used for each channel and a full *z*-stack of the cluster was produced. Images were then subjected to 3D reconstruction

678 through the "3D Project" function in FIJI. Border cell-border cell (BC-BC) contacts and nurse
679 cell-nurse cell (NC-NC) contacts were manually identified, a line (width set as 6) drawn, and
680 mean fluorescence intensity across the line was obtained using the "measure" tool. A ratio of
681 BC-BC intensity versus NC-NC intensity was calculated to normalize protein levels.
682 To measure colocalization between Mbs and Flw, or Mbs and Pp1α-96A, the "RGB
683 Profiler" FIJI plugin was used. After converting the image to RGB, a line was drawn across the
684 whole border cell cluster to generate the image intensity plot. The localization patterns of F-actin
685 and Mbs with Pp1α-96A-GFP and Flw-YFP were measured through the "Analyze>Plot Profile"
686 function in FIJI. A line was drawn across the border cells and polar cells and the pixel intensity
687 value was obtained across the line. The values for each channel were normalized to the highest
688 pixel value, and a scatter plot showing F-actin and DAPI was generated in Microsoft Excel.
689 For Rho-FRET and Rac-FRET, the CFP and YFP images were first processed in ImageJ.
690 A background region of interest was subtracted from the original image. The YFP images were
691 registered to CFP images using the TurboReg plugin. The Gaussian smooth filter was then
692 applied to both channels. The YFP image was thresholded and converted to a binary mask with
693 the background set to zero. The final ratio image was generated in MATLAB, during which only
694 the unmasked pixels were calculated as described[22].
695
696 **Figures, graphs, and statistics**
697 Figures were assembled in Adobe Photoshop CC. Illustrations were created in Affinity Designer
698 (Serif, Nottingham, United Kingdom). Videos were assembled in Zeiss AxioVision 4.8, Zeiss
699 ZEN 2, or FIJI. Graphs and statistical tests were performed using GraphPad Prism 7 (GraphPad
700 Software, San Diego, CA, USA). The statistical tests and *p* values are listed in the figure legends.

Acknowledgements

We thank Drs. Chris Doe, Denise Montell, Pernille Rørth, Change Tan, Tina Tootle, Alan Zhu, the Bloomington *Drosophila* Stock Center, the Developmental Studies Hybridoma Center (University of Iowa), FlyORF, the Kyoto Stock Center, and Vienna Drosophila Resource Center (VDRC) for fly stocks, antibodies, and protocols. We also thank Dr. Pralay Majumder for discussions and providing comments on the manuscript. The Confocal Core, funded by the Kansas State University College of Veterinary Medicine, provided use of the Zeiss LSM 880 confocal microscope. This work was supported in part by a fellowship from the Kansas INBRE through the National Institutes of Health (P20 GM103418) to Y.C., and by grants from the Scientifiques de la Fondation ARC (grant number PJA 20171206526) to X.W. and the National Science Foundation (1456053 and 1738757) to J.A.M.

References

1. Friedl, P., Locker, J., Sahai, E. & Segall, J. E. Classifying collective cancer cell invasion. *Nat. Cell Biol.* **14,** 777–783 (2012).
2. Friedl, P. & Gilmour, D. Collective cell migration in morphogenesis, regeneration and cancer. *Nat. Rev. Mol. Cell Biol.* **10,** 445–457 (2009).
3. Wang, X., Enomoto, A., Asai, N., Kato, T. & Takahashi, M. Collective invasion of cancer: Perspectives from pathology and development. *Pathol. Int.* **66,** 183–192 (2016).
4. Cheung, K. J. & Ewald, A. J. A collective route to metastasis: Seeding by tumor cell clusters. *Science* **352,** 167–169 (2016).
5. Scarpa, E. & Mayor, R. Collective cell migration in development. *J. Cell Biol.* **212,** 143–155 (2016).
6. Huebner, R. J., Neumann, N. M. & Ewald, A. J. Mammary epithelial tubes elongate through MAPK-dependent coordination of cell migration. *Development* **143,** 983–993 (2016).
7. Shellard, A. & Mayor, R. Supracellular migration - beyond collective cell migration. *J. Cell Sci.* **132,** jcs226142 (2019).
8. Mayor, R. & Etienne-Manneville, S. The front and rear of collective cell migration. *Nat. Rev. Mol. Cell Biol.* **17,** 97–109 (2016).
9. Friedl, P. & Mayor, R. Tuning Collective Cell Migration by Cell-Cell Junction Regulation. *Cold Spring Harb. Perspect. Biol.* **9,** a029199 (2017).
10. Shellard, A., Szabó, A., Trepat, X. & Mayor, R. Supracellular contraction at the rear of neural crest cell groups drives collective chemotaxis. *Science* **362,** 339–343 (2018).
11. Hidalgo-Carcedo, C., Hooper, S., Chaudhry, S. I., Williamson, P., Harrington, K., Leitinger, B. & Sahai, E. Collective cell migration requires suppression of actomyosin at cell-cell contacts mediated by DDR1 and the cell polarity regulators Par3 and Par6. *Nat. Cell Biol.* **13,** 49–58 (2011).
12. Reffay, M., Parrini, M. C., Cochet-Escartin, O., Ladoux, B., Buguin, A., Coscoy, S., Amblard, F., Camonis, J. & Silberzan, P. Interplay of RhoA and mechanical forces in collective cell migration driven by leader cells. *Nat. Cell Biol.* **16,** 217–223 (2014).
13. Montell, D. J., Yoon, W. H. & Starz-Gaiano, M. Group choreography: mechanisms orchestrating the collective movement of border cells. *Nat. Rev. Mol. Cell Biol.* **13,** 631–645 (2012).
14. Saadin, A. & Starz-Gaiano, M. Circuitous Genetic Regulation Governs a Straightforward Cell Migration. *Trends Genet.* **32,** 660–673 (2016).
15. Llense, F. & Martín-Blanco, E. JNK signaling controls border cell cluster integrity and collective cell migration. *Curr. Biol.* **18,** 538–544 (2008).
16. Cai, D., Chen, S.-C., Prasad, M., He, L., Wang, X., Choesmel-Cadamuro, V., Sawyer, J. K., Danuser, G. & Montell, D. J. Mechanical Feedback through E-Cadherin Promotes Direction Sensing during Collective Cell Migration. *Cell* **157,** 1146–1159 (2014).
17. Prasad, M. & Montell, D. J. Cellular and Molecular Mechanisms of Border Cell Migration Analyzed Using Time-Lapse Live-Cell Imaging. *Dev. Cell* **12,** 997–1005 (2007).
18. Bianco, A., Poukkula, M., Cliffe, A., Mathieu, J., Luque, C. M., Fulga, T. A. & Rørth, P. Two distinct modes of guidance signalling during collective migration of border cells. *Nature* **448,** 362–365 (2007).
19. Poukkula, M., Cliffe, A., Changede, R. & Rørth, P. Cell behaviors regulated by guidance cues in collective migration of border cells. *J. Cell Biol.* **192,** 513–524 (2011).
20. Duchek, P., Somogyi, K., Jékely, G., Beccari, S. & Rørth, P. Guidance of cell migration by the Drosophila PDGF/VEGF receptor. *Cell* **107,** 17–26 (2001).
21. McDonald, J. A., Pinheiro, E. M., Kadlec, L., Schupbach, T. & Montell, D. J. Multiple EGFR ligands participate in guiding migrating border cells. *Dev. Biol.* **296,** 94–103 (2006).

22. Wang, X., He, L., Wu, Y. I., Hahn, K. M. & Montell, D. J. Light-mediated activation reveals a key role for Rac in collective guidance of cell movement in vivo. *Nat. Cell Biol.* **12,** 591–597 (2010).
23. Ramel, D., Wang, X., Laflamme, C., Montell, D. J. & Emery, G. Rab11 regulates cell-cell communication during collective cell movements. *Nat. Cell Biol.* **15,** 317–324 (2013).
24. Aranjuez, G., Burtscher, A., Sawant, K., Majumder, P. & McDonald, J. A. Dynamic myosin activation promotes collective morphology and migration by locally balancing oppositional forces from surrounding tissue. *Mol. Biol. Cell* **27,** 1898–1910 (2016).
25. Lucas, E. P., Khanal, I., Gaspar, P., Fletcher, G. C., Polesello, C., Tapon, N. & Thompson, B. J. The Hippo pathway polarizes the actin cytoskeleton during collective migration of Drosophila border cells. *J. Cell Biol.* **201,** 875–885 (2013).
26. Combedazou, A., Choesmel-Cadamuro, V., Gay, G., Liu, J., Dupré, L., Ramel, D. & Wang, X. Myosin II governs collective cell migration behaviour downstream of guidance receptor signalling. *J. Cell Sci.* **130,** 97–103 (2017).
27. Larsen, M., Tremblay, M. L. & Yamada, K. M. Phosphatases in cell–matrix adhesion and migration. *Nat. Rev. Mol. Cell Biol.* **4,** 700–711 (2003).
28. Majumder, P., Aranjuez, G., Amick, J. & McDonald, J. A. Par-1 controls myosin-II activity through myosin phosphatase to regulate border cell migration. *Curr. Biol.* **22,** 363–372 (2012).
29. Felix, M., Chayengia, M., Ghosh, R., Sharma, A., & Prasad, M. Pak3 regulates apical-basal polarity in migrating border cells during Drosophila oogenesis. *Development* **142,** 3692–3703 (2015).
30. Lin, Q., Buckler, E. S., Muse, S. V. & Walker, J. C. Molecular evolution of type 1 serine/threonine protein phosphatases. *Mol. Phylogenet. Evol.* **12,** 57–66 (1999).
31. Verbinnen, I., Ferreira, M. & Bollen, M. Biogenesis and activity regulation of protein phosphatase 1. *Biochem. Soc. Trans.* **45,** 89–99 (2017).
32. Heroes, E., Lesage, B., Görnemann, J., Beullens, M., Van Meervelt, L. & Bollen, M. The PP1 binding code: a molecular-lego strategy that governs specificity. *FEBS J.* **280,** 584–595 (2013).
33. Ceulemans, H. & Bollen, M. Functional diversity of protein phosphatase-1, a cellular economizer and reset button. *Physiol. Rev.* **84,** 1–39 (2004).
34. Ferreira, M., Beullens, M., Bollen, M. & Van Eynde, A. Functions and therapeutic potential of protein phosphatase 1: Insights from mouse genetics. *Biochim. Biophys. Acta Mol. Cell Res.* **1866,** 16–30 (2019).
35. Miskei, M., Ádám, C., Kovács, L., Karányi, Z. & Dombrádi, V. Molecular Evolution of Phosphoprotein Phosphatases in Drosophila. *PLoS ONE* **6,** e22218 (2011).
36. Bennett, D., Szöor, B., Gross, S., Vereshchagina, N. & Alphey, L. Ectopic expression of inhibitors of protein phosphatase type 1 (PP1) can be used to analyze roles of PP1 in Drosophila development. *Genetics* **164,** 235–245 (2003).
37. Winkler, C., De Munter, S., Van Dessel, N., Lesage, B., Heroes, E., Boens, S., Beullens, M., Van Eynde, A. & Bollen, M. The selective inhibition of protein phosphatase-1 results in mitotic catastrophe and impaired tumor growth. *J. Cell Sci.* **128,** 4526–4537 (2015).
38. Parker, L., Gross, S., Beullens, M., Bollen, M., Bennett, D. & Alphey, L. Functional interaction between nuclear inhibitor of protein phosphatase type 1 (NIPP1) and protein phosphatase type 1 (PP1) in Drosophila: consequences of over-expression of NIPP1 in flies and suppression by co-expression of PP1. *Biochem. J.* **368,** 789–797 (2002).
39. Van Eynde, A., Wera, S., Beullens, M., Torrekens, S., Van Leuven, F., Stalmans, W. & Bollen, M. Molecular Cloning of NIPP-1, a Nuclear Inhibitor of Protein Phosphatase-1, Reveals Homology with Polypeptides Involved in RNA Processing. *J. Biol. Chem.* **270,** 28068–28074 (1995).

40. Silver, D. L. & Montell, D. J. Paracrine Signaling through the JAK/STAT Pathway Activates Invasive Behavior of Ovarian Epithelial Cells in Drosophila. *Cell* **107,** 831–841 (2001).
41. Niewiadomska, P., Godt, D. & Tepass, U. DE-Cadherin is required for intercellular motility during Drosophila oogenesis. *J. Cell Biol.* **144,** 533–547 (1999).
42. Montell, D. J., Rørth, P. & Spradling, A. C. slow border cells, a locus required for a developmentally regulated cell migration during oogenesis, encodes Drosophila CEBP. *Cell* **71,** 51–62 (1992).
43. Starz-Gaiano, M., Melani, M., Wang, X., Meinhardt, H. & Montell, D. J. Feedback inhibition of Jak/STAT signaling by apontic is required to limit an invasive cell population. *Dev. Cell* **14,** 726–738 (2008).
44. Dai, W. & Montell, D. J. Live Imaging of Border Cell Migration in Drosophila. *Methods Mol. Biol.* **1407,** 153–168 (2016).
45. Dombrádi, V., Mann, D. J., Saunders, R. D. C. & Cohen, P. T. W. Cloning of the fourth functional gene for Protein Phosphatase 1 in Drosophila melanogaster from its chromosomal location. *Eur. J. Biochem.* **212,** 177–183 (1993).
46. Dombrádi, V., Axton, J. M., Brewis, N. D., Silva, E. F. D. C. E., Alphey, L. & Cohen, P. T. W. Drosophila contains three genes that encode distinct isoforms of protein phosphatase 1. *Eur. J. Biochem.* **194,** 739–745 (1990).
47. Graveley, B. R., Brooks, A. N., Carlson, J. W., Duff, M. O., Landolin, J. M., Yang, L., Artieri, C. G., van Baren, M. J., Boley, N., Booth, B. W., Brown, J. B., Cherbas, L., Davis, C. A., Dobin, A., Li, R., Lin, W., Malone, J. H., Mattiuzzo, N. R., Miller, D., Sturgill, D., Tuch, B. B., Zaleski, C., Zhang, D., Blanchette, M., Dudoit, S., Eads, B., Green, R. E., Hammonds, A., Jiang, L., Kapranov, P., Langton, L., Perrimon, N., Sandler, J. E., Wan, K. H., Willingham, A., Zhang, Y., Zou, Y., Andrews, J., Bickel, P. J., Brenner, S. E., Brent, M. R., Cherbas, P., Gingeras, T. R., Hoskins, R. A., Kaufman, T. C., Oliver, B. & Celniker, S. E. The developmental transcriptome of Drosophila melanogaster. *Nature* **471,** 473–479 (2011).
48. Sarov, M., Barz, C., Jambor, H., Hein, M. Y., Schmied, C., Suchold, D., Stender, B., Janosch, S., Kj, V. V., Krishnan, R. T., Krishnamoorthy, A., Ferreira, I. R., Ejsmont, R. K., Finkl, K., Hasse, S., Kämpfer, P., Plewka, N., Vinis, E., Schloissnig, S., Knust, E., Hartenstein, V., Mann, M., Ramaswami, M., VijayRaghavan, K., Tomancak, P. & Schnorrer, F. A genome-wide resource for the analysis of protein localisation in Drosophila. *Elife* **5,** e12068 (2016).
49. Yamamoto, S., Bayat, V., Bellen, H. J. & Tan, C. Protein Phosphatase 1ß Limits Ring Canal Constriction during Drosophila Germline Cyst Formation. *PLoS ONE* **8,** e70502 (2013).
50. Hu, Y., Flockhart, I., Vinayagam, A., Bergwitz, C., Berger, B., Perrimon, N. & Mohr, S. E. An integrative approach to ortholog prediction for disease-focused and other functional studies. *BMC Bioinformatics* **12,** 357–1100 (2011).
51. Trinkle-Mulcahy, L., Sleeman, J. E. & Lamond, A. I. Dynamic targeting of protein phosphatase 1 within the nuclei of living mammalian cells. *J. Cell Sci.* **114,** 4219–4228 (2001).
52. Mohr, S. E., Smith, J. A., Shamu, C. E., Neumüller, R. A. & Perrimon, N. RNAi screening comes of age: improved techniques and complementary approaches. *Nat. Rev. Mol. Cell Biol.* **15,** 591–600 (2014).
53. Sun, Y., Yan, Y., Denef, N. & Schupbach, T. Regulation of somatic myosin activity by protein phosphatase 1β controls Drosophila oocyte polarization. *Development* **138,** 1991–2001 (2011).
54. Collins, C. & Nelson, W. J. Running with neighbors: coordinating cell migration and cell–cell adhesion. *Curr. Opin. Cell Biol.* **36,** 62–70 (2015).

55. Sarpal, R., Pellikka, M., Patel, R. R., Hui, F. Y. W., Godt, D. & Tepass, U. Mutational analysis supports a core role for Drosophila α-catenin in adherens junction function. *J. Cell Sci.* **125,** 233–245 (2012).
56. Desai, R., Sarpal, R., Ishiyama, N., Pellikka, M., Ikura, M. & Tepass, U. Monomeric α-catenin links cadherin to the actin cytoskeleton. *Nat. Cell Biol.* **15,** 261–273 (2013).
57. Pacquelet, A. & Rørth, P. Regulatory mechanisms required for DE-cadherin function in cell migration and other types of adhesion. *J. Cell Biol.* **170,** 803–812 (2005).
58. Ridley, A. J. Life at the leading edge. *Cell* **145,** 1012–1022 (2011).
59. Caswell, P. T. & Zech, T. Actin-Based Cell Protrusion in a 3D Matrix. *Trends Cell Biol.* **28,** 823–834 (2018).
60. Boekhorst, Te, V., Preziosi, L. & Friedl, P. Plasticity of Cell Migration In Vivo and In Silico. *Annu. Rev. Cell Dev. Biol.* **32,** 491–526 (2016).
61. Wang, H., Qiu, Z., Xu, Z., Chen, S. J., Luo, J., Wang, X. & Chen, J. aPKC is a key polarity determinant in coordinating the function of three distinct cell polarities during collective migration. *Development* **145,** dev158444 (2018).
62. Vicente-Manzanares, M., Ma, X., Adelstein, R. S. & Horwitz, A. R. Non-muscle myosin II takes centre stage in cell adhesion and migration. *Nat. Rev. Mol. Cell Biol.* **10,** 778–790 (2009).
63. Grassie, M. E., Moffat, L. D., Walsh, M. P. & MacDonald, J. A. The myosin phosphatase targeting protein (MYPT) family: a regulated mechanism for achieving substrate specificity of the catalytic subunit of protein phosphatase type 1δ. *Arch. Biochem. Biophys.* **510,** 147–159 (2011).
64. Qin, X., Park, B. O., Liu, J., Chen, B., Choesmel-Cadamuro, V., Belguise, K., Do Heo, W. & Wang, X. Cell-matrix adhesion and cell-cell adhesion differentially control basal myosin oscillation and Drosophila egg chamber elongation. *Nat. Comm.* **8,** 14708 (2017).
65. Fulga, T. A. & Rørth, P. Invasive cell migration is initiated by guided growth of long cellular extensions. *Nat. Cell Biol.* **4,** 715–719 (2002).
66. Kimura, K., Ito, M., Amano, M., Chihara, K., Fukata, Y., Nakafuku, M., Yamamori, B., Feng, J., Nakano, T., Okawa, K., Iwamatsu, A. & Kaibuchi, K. Regulation of myosin phosphatase by Rho and Rho-associated kinase (Rho-kinase). *Science* **273,** 245–248 (1996).
67. Amano, M., Ito, M., Kimura, K., Fukata, Y., Chihara, K., Nakano, T., Matsuura, Y. & Kaibuchi, K. Phosphorylation and activation of myosin by Rho-associated kinase (Rho-kinase). *J. Biol. Chem.* **271,** 20246–20249 (1996).
68. Matsui, T., Amano, M., Yamamoto, T., Chihara, K., Nakafuku, M., Ito, M., Nakano, T., Okawa, K., Iwamatsu, A. & Kaibuchi, K. Rho-associated kinase, a novel serine/threonine kinase, as a putative target for small GTP binding protein Rho. *EMBO J.* **15,** 2208–2216 (1996).
69. Julian, L. & Olson, M. F. Rho-associated coiled-coil containing kinases (ROCK). *Small GTPases* **5,** e29846 (2014).
70. Bravo-Cordero, J. J., Magalhaes, M. A. O., Eddy, R. J., Hodgson, L. & Condeelis, J. Functions of cofilin in cell locomotion and invasion. *Nat. Rev. Mol. Cell Biol.* **14,** (2013).
71. Zhang, L., Luo, J., Wan, P., Wu, J., Laski, F. & Chen, J. Regulation of cofilin phosphorylation and asymmetry in collective cell migration during morphogenesis. *Development* **138,** 455–464 (2011).
72. Huet, G., Rajakylä, E. K., Viita, T., Skarp, K.-P., Crivaro, M., Dopie, J. & Vartiainen, M. K. Actin-regulated feedback loop based on Phactr4, PP1 and cofilin maintains the actin monomer pool. *J. Cell Sci.* **126,** 497–507 (2013).
73. Ambach, A., Saunus, J., Konstandin, M., Wesselborg, S., Meuer, S. C. & Samstag, Y. The serine phosphatases PP1 and PP2A associate with and activate the actin-binding protein cofilin in human T lymphocytes. *Eur. J. Immunol.* **30,** 3422–3431 (2000).

74. Zhang, Y., Kim, T.-H. & Niswander, L. Phactr4 regulates directional migration of enteric neural crest through PP1, integrin signaling, and cofilin activity. *Genes Dev.* **26,** 69–81 (2012).
75. Oleinik, N. V., Krupenko, N. I. & Krupenko, S. A. ALDH1L1 inhibits cell motility via dephosphorylation of cofilin by PP1 and PP2A. *Oncogene* **29,** 6233–6244 (2010).
76. Kühn, S. & Geyer, M. Formins as effector proteins of Rho GTPases. *Small GTPases* **5,** e983876 (2014).
77. Stappert, J. & Kemler, R. A short core region of E-cadherin is essential for catenin binding and is highly phosphorylated. *Cell Adhes. Commun.* **2,** 319–327 (1994).
78. McEwen, A. E., Maher, M. T., Mo, R. & Gottardi, C. J. E-cadherin phosphorylation occurs during its biosynthesis to promote its cell surface stability and adhesion. *Mol. Biol. Cell* **25,** 2365–2374 (2014).
79. Chen, Y.-J., Huang, J., Huang, L., Austin, E. & Hong, Y. Phosphorylation potential of Drosophila E-Cadherin intracellular domain is essential for development and adherens junction biosynthetic dynamics regulation. *Development* **144,** 1242–1248 (2017).
80. Escobar, D. J., Desai, R., Ishiyama, N., Folmsbee, S. S., Novak, M. N., Flozak, A. S., Daugherty, R. L., Mo, R., Nanavati, D., Sarpal, R., Leckband, D., Ikura, M., Tepass, U. & Gottardi, C. J. α-Catenin phosphorylation promotes intercellular adhesion through a dual-kinase mechanism. *J. Cell Sci.* **128,** 1150–1165 (2015).
81. Yap, A. S., Duszyc, K. & Viasnoff, V. Mechanosensing and Mechanotransduction at Cell-Cell Junctions. *Cold Spring Harb. Perspect. Biol.* a028761 (2017).
82. Mège, R.-M. & Ishiyama, N. Integration of Cadherin Adhesion and Cytoskeleton at AdherensJunctions. *Cold Spring Harb. Perspect. Biol.* **9,** a028738 (2017).
83. Weiser, D. C., Row, R. H. & Kimelman, D. Rho-regulated Myosin phosphatase establishes the level of protrusive activity required for cell movements during zebrafish gastrulation. *Development* **136,** 2375–2384 (2009).
84. McGuire, S. E., Mao, Z. & Davis, R. L. Spatiotemporal Gene Expression Targeting with the TARGET and Gene-Switch Systems in Drosophila. *Sci. Signal.* **2004,** pl6 (2004).
85. Rørth, P., Szabo, K., Bailey, A., Laverty, T., Rehm, J., Rubin, G. M., Weigmann, K., Milán, M., Benes, V., Ansorge, W. & Cohen, S. M. Systematic gain-of-function genetics in Drosophila. *Development* **125,** 1049–1057 (1998).
86. Xu, T. & Rubin, G. M. Analysis of genetic mosaics in developing and adult Drosophila tissues. *Development* **117,** 1223–1237 (1993).
87. Bischof, J., Björklund, M., Furger, E., Schertel, C., Taipale, J. & Basler, K. A versatile platform for creating a comprehensive UAS-ORFeome library in Drosophila. *Development* **140,** 2434–2442 (2013).
88. Tootle, T. L. & Spradling, A. C. Drosophila Pxt: a cyclooxygenase-like facilitator of follicle maturation. *Development* **135,** 839–847 (2008).
89. Spracklen, A. J., Kelpsch, D. J., Chen, X., Spracklen, C. N. & Tootle, T. L. Prostaglandins temporally regulate cytoplasmic actin bundle formation during Drosophila oogenesis. *Mol. Biol. Cell* **25,** 397–411 (2014).
90. Schindelin, J., Arganda-Carreras, I., Frise, E., Kaynig, V., Longair, M., Pietzsch, T., Preibisch, S., Rueden, C., Saalfeld, S., Schmid, B., Tinevez, J.-Y., White, D. J., Hartenstein, V., Eliceiri, K., Tomancak, P. & Cardona, A. Fiji: an open-source platform for biological-image analysis. *Nat. Methods* **9,** 676–682 (2012).
91. Sawant, K., Chen, Y., Kotian, N., Preuss, K. M. & McDonald, J. A. Rap1 GTPase promotes coordinated collective cell migration in vivo. *Mol. Biol. Cell* **29,** 2656–2673 (2018).
92. Jambor, H., Surendranath, V., Kalinka, A. T., Mejstrik, P., Saalfeld, S. & Tomancak, P. Systematic imaging reveals features and changing localization of mRNAs in Drosophila development. *Elife* **4,** R106 (2015).

Figure Legends

Figure 1

NiPp1 expression causes the border cell cluster to fall apart and disrupts migration. (**A-F**) Wild-type border cell migration during oogenesis stages 9 and 10. (**A-C**) Egg chambers at the indicated stages labeled with E-Cadherin (E-Cad; green), F-actin (magenta) and DAPI (blue). Arrowheads indicate the border cell cluster. (**D-F**) Magnified views of the same border cell cluster from (A-C), showing FasIII (red) in the polar cells, E-Cad and DAPI. The border cell cluster is composed of two polar cells (marked by asterisks) in the center and four to eight outer border cells that are tightly connected with each other as indicated by E-Cad staining. (**G, H**) Egg chambers labeled with Singed (SN; green) to detect border cells (arrowheads), phalloidin to detect F-actin (red), and DAPI to detect nuclei (blue). Control border cells (G) reach the oocyte as a single cluster, whereas NiPp1-expressing border cells (H) dissociate from the cluster into small groups, with only a few reaching the oocyte. (**I**) Quantification of border cell cluster migration for matched control and NiPp1 overexpression, shown as the percentage that did not complete (red), or completed (green) their migration to the oocyte, as indicated in the egg chamber schematic. (**J**) Quantification of cluster cohesion, shown as the percentage of border cells found as a single unit (1 part) or split into multiple parts (2-3 parts or >3 parts) in control versus NiPp1-expressing egg chambers. (**I, J**) Error bars represent SEM in 3 experiments, each trial assayed n ≥ 69 egg chambers (total n ≥ 221 egg chambers per genotype). ***p < 0.001, ****p < 0.0001, unpaired two-tailed *t* test. (**K-L''**) Frames from a control (Video 1; K-K") and an NiPp1 overexpression (OE; Video 2; L-L") time-lapse video showing movement of the border cell cluster over the course of 3 h (time in minutes). Border cells (arrowheads) express UAS-mCherry-Jupiter, which labels cytoplasmic microtubules. (**M**) Measurement of border cell migration speed from control (n=11 videos) and NiPp1 overexpression (n=11 videos; 22 tracked border cell 'parts') videos, shown as a box-and-whiskers plot. The whiskers represent the minimum and maximum pixel intensity; the box extends from the 25th to the 75th percentiles and the line indicates the median. ****p < 0.0001, unpaired two-tailed *t* test. In this and all subsequent figures, anterior is to the left and the scale bars indicate the image magnification. All genotypes are listed in Supplemental Table 2.

Figure 2

Pp1c expression in border cells and specificity of Pp1c activity inhibition by NiPp1. (**A-F**) Stage 9 and 10 egg chambers showing the endogenous patterns of Pp1c subunits (green) in border cells (arrowheads), follicle cells, and the germline nurse cells and oocyte. DAPI (blue) labels nuclei. Insets, zoomed-in detail of border cells from the same egg chambers. (**A-C**) Pp1α-96A (green) expression, visualized by a GFP-tagged fly-TransgeneOme (fTRG) line. (**D-F**) Flw expression (green), visualized by a YFP-protein trap in the endogenous *flw* genetic locus. (**G, H**) Overexpression of *Pp1c* genes rescues the migration (G) and cluster cohesion (H) defects of NiPp1-expressing border cells. (**G**) Quantification of the migration distance at stage 10 for border cells in NiPp1-expressing egg chambers versus rescue by overexpression of the indicated *Pp1c* genes, shown as complete (green) and incomplete (red) border cell migration (see Figure 1I for egg chamber schematic). (**H**) Quantification of cluster cohesion at stage 10, shown as the percentage of border cells found as a single unit (1 part) or split into multiple parts

(2 parts, 3 parts, >3 parts) in NiPp1-expressing egg chambers versus rescue by overexpression of the indicated *Pp1c* genes. (**G, H**) Error bars represent SEM in 3 experiments, each trial assayed n ≥ 44 egg chambers (total n ≥ 148 per genotype). *p < 0.05, **p < 0.01; ***p < 0.001; ****p < 0.0001, unpaired two-tailed *t* test. All genotypes are listed in Supplemental Table 2.

Figure 3

Pp1c genes are required for normal border cell migration and cluster cohesion. (**A-F**) Knockdown of *Pp1c* genes by RNAi disrupts border cell cluster migration and cohesion. (**A-D**) Stage 10 egg chambers expressing RNAi against the indicated genes were stained for SN (red) to label border cells (arrowheads), phalloidin to label F-actin (green) and DAPI to label nuclei (blue). (**E**) Quantification of border cell cluster migration for matched control and RNAi knockdown of the indicated *Pp1c* genes, shown as the percentage that did not complete (red), or completed (green) their migration to the oocyte (see Figure 1I for egg chamber schematic). (**F**) Quantification of cluster cohesion, shown as the percentage of border cells found as a single unit (1 part) or split into multiple parts (2-3 parts or >3 parts) in control versus *Pp1c* RNAi egg chambers. (**E, F**) Error bars represent SEM in 3 experiments, each trial assayed n ≥ 59 (total n ≥ 246 per genotype). (**G**) Measurement of border cell migration speed in the indicated genotypes from individual videos of *Pp1c* RNAi border cells; n=14 videos for control, n=11 videos for *Pp1-87B-RNAi* (27 split parts were tracked), n=12 videos for *Pp1-13C-RNAi* (17 split parts were tracked), n=16 videos for *Pp1alpha-96A-RNAi* (38 split parts were tracked), box-and-whiskers plot (see Figure 1 legend for details of plot). (**E-G**) *p < 0.05, **p < 0.01, ***p < 0.001, ****p < 0.0001, unpaired two-tailed *t* test. (**H-J**) *flw* mutant border cells split from the cluster and often fail to migrate. (**H-H''**) Representative image of a stage 10 egg chamber with flw^{FP41} mutant clones, marked by the loss of nuclear mRFP (dotted outline in H, H') and stained for SN (green in H") to mark border cells (arrowheads) and DAPI (blue in H) to mark nuclei. (**I, J**) Quantification of flw^{FP41} mutant cluster cohesion (I) and migration (J) at stage 10; n=20 egg chambers with flw^{FP41} clones were examined. (**I**) Quantification of cluster cohesion at stage 10, shown as the percentage of flw^{FP41} mosaic border cells found as a single unit (1 part) or split into multiple parts (2, 3, or 4 parts). (**J**) Quantification of the migration distance at stage 10 for flw^{FP41} mosaic mutant border cells, shown as complete (green), partial (blue), or incomplete (red) border cell migration. All genotypes are listed in Supplemental Table 2.

Figure 4

The cadherin-catenin complex is required for the collective cohesion of the migrating border cell cluster and is regulated by Pp1. (**A-J**) Knocking down *E-Cad*, *β-Cat* or *α-Cat* by RNAi disrupts border cell cluster migration and cohesion. Images of stage 10 egg chambers stained for phalloidin to label F-actin (red) and DAPI to label nuclei (blue). Border cells (arrowheads) express the membrane marker PLC∂-PH-GFP (green). (**E-J**) Quantification of border cell migration (E, G, I) and cluster cohesion (F, H, J) in stage 10 control and *E-Cad-RNAi* (E, F), *β-Cat-RNAi* (G, H) *and α-Cat-RNAi* (I, J) egg chambers. The controls for *E-Cad* and *β-Cat-RNAi* are identical, but shown on separate graphs (E-H) for clarity; a separate matched control is shown for *α-Cat* RNAi (I, J). Error bars represent SEM in 3 experiments, each trial assayed n ≥ 27 egg chambers (total n ≥ 93 for *each genotype*). *p < 0.05; **p < 0.01; ***p < 0.001; ****p < 0.0001, unpaired two-tailed *t* test. (**E, G, I**) Quantification of border cell migration, shown as the percentage of egg chambers with complete (green), partial (blue), or no (red), border cell

migration. (**F, H, J**) Quantification of cluster cohesion, shown as the percentage of border cells found as a single unit (1 part) or split into multiple parts (2-3 parts or >3 parts) in control versus RNAi egg chambers. (**K-N''**) Representative images showing the E-Cad (white in K, L; green in K", L") and β-cat (white in M, N; green in M", N") protein expression pattern in control and NiPp1 overexpressing (OE) border cells. Border cells were co-stained for DAPI to mark nuclei (white in K', L', M', N'; blue in K", L", M", N"). Images were generated from merged *z*-sections. The enriched levels of E-Cad (K, L) and β-cat (M, N) between border cells (border cell-border cell contacts) are marked by yellow and magenta arrows, respectively. The central polar cells are indicated by red arrowheads (K', L', M', N'). (**O, P**) Quantification of relative E-Cad (O) and β-Cat (P) protein intensity levels in control and NiPp1 overexpressing border cell clusters shown as box-and-whiskers plots (see Figure 1 legend for details of plot). For E-Cad, 39 border cell-border cell contacts from 8 matched control clusters and 24 border cell-border cell contacts from 16 NiPp1 clusters were measured. For β-Cat, 33 border cell-border cell contacts from 7 matched control clusters and 23 border cell-border cell contacts from 15 NiPp1 clusters were measured. ***p < 0.001, ****p < 0.0001, unpaired two-tailed *t* test. All genotypes are listed in Supplemental Table 2.

Figure 5

Pp1c is required for normal border cell protrusion dynamics. (**A-B""**) Frames from a matched control (Video 6; A-A"") and a *Pp1alpha-96A-RNAi* (Video 7; B-B"") showing the migrating border cell cluster expressing the membrane marker PLC∂-PH-GFP. Time in min. Arrows indicate protrusions, arrowheads indicate cluster "parts". (**C-F**) Quantification of the number of protrusions per frame (C), average protrusion lifetime (D), average protrusion length (E), and average protrusion area (F) from videos of the indicated genotypes. Protrusions were defined as in Supplemental Figure 6A and in the Materials and Methods. For control, protrusions were measured in 14 videos (n=51 front-directed protrusions, n=15 side-directed protrusions, n=2 back-directed protrusions); for *Pp1alpha-96A-RNAi*, protrusions were measured in n=16 videos (n=59 front protrusions, n=19 side protrusions, n=9 for back protrusions), for *Pp1-87B-RNAi*, protrusions were measured in 13 videos (n=67 for front protrusions, n=10 for side protrusions, n=3 for back protrusions)*;* for *Pp1-13C-RNAi*, protrusions were measured in 12 videos (n=61 front protrusions, n=9 side protrusions, n=1 back protrusion). Data are presented as box-and-whiskers plots (see Figure 1 legend for details of plot). *p < 0.05, **p < 0.01, ***p < 0.001, ****p < 0.0001, unpaired two-tailed *t* test. All genotypes are listed in Supplemental Table 2.

Figure 6

Pp1 activity promotes normal border cell shape and distribution of actomyosin in the border cell cluster. (**A-C**) Pp1 is required for border cell shape. (**A-B'**) Examples of control (A, A') and NiPp1-expressing border cells (B, B'). Cell shape was visualized using the membrane marker PLC∂-PH-GFP driven by *slbo*-GAL4 (green). Cells were outlined (A, B) and measured for circularity (C). (**C**) Control border cells are more elongated compared to NiPp1-expressing border cells (closer to 1.0, a perfect circle). Quantification of circularity, showing all data points and the mean; 51 control border cells and 57 NiPp1-expressing border cells were measured. ****p < 0.0001, unpaired two-tailed *t* test. (**D-G**) Pp1 restricts high levels of F-actin to the border cell cluster periphery. Egg chambers were stained for phalloidin to detect F-actin (green in D, E; white in D', E') and DAPI to visualize nuclei (white in D, E). (**D, D'**) Control wild-type border cells

(w^{1118}) have higher F-actin at the cluster perimeter (magenta arrows) and low levels at cell-cell contacts inside the cluster (yellow arrows). (**E, E'**) NiPp1 overexpression increases F-actin inside the cluster at cell contacts between border cells and at cell contacts between polar cells and border cells (yellow arrows). F-actin is relatively high on the outer surfaces of border cells (magenta arrows). (**F, G**) Plot profiles of normalized F-actin (orange) and DAPI (blue) fluorescence pixel intensity (AU, arbitrary units) measured along the lines shown in (D) and (E); similar results were obtained from additional border cell clusters (n=11 for control and n=8 for *slbo*>NiPp1). (**H-H''''**) Pp1 restricts Myo-II, as visualized by Sqh:GFP, to the cluster periphery in live border cells. Stills from confocal videos of Sqh:GFP in early-staged border cells over the course of 5 minutes. (**H-H''''**) Control border cells (video 13; w^{1118}). (**I-I''''**) NiPp1 overexpression (video 14) changes the dynamics of Sqh:GFP, with more Sqh:GFP located at cell contacts between border cells. All genotypes are listed in Supplemental Table 2.

Figure 7

Pp1, through myosin phosphatase, promotes contractility of the cluster. (**A-B'**) Pp1 restricts Myo-II activation to the cluster periphery. Representative images showing p-Sqh localization (green in A, B; white in A', B') in control (A-A') and NiPp1 overexpressing (B-B') border cells; DAPI labels nuclei (blue in A, B). (**C-F**) Knocking down *Mbs* disrupts border cell migration and cluster cohesion. (**C, D**) Stage 10 control (C) and *Mbs* RNAi (D) egg chambers stained for SN to label border cells (green), phalloidin to label F-actin (red) and DAPI to label nuclei (blue). (**E**) Quantification of border cell cluster migration for matched control and *Mbs-RNAi*, shown as the percentage that did not complete (red), or completed (green) their migration to the oocyte (see Figure 1I for egg chamber schematic). (**F**) Quantification of cluster cohesion at stage 10, shown as the percentage of border cells found as a single unit (1 part) or split into multiple parts (2 parts, 3 parts, >3 parts) in control versus *Mbs-RNAi* border cells. (**E, F**) Each trial assayed n ≥ 61 egg chambers (total n ≥ 220 per genotype). **p < 0.01; ****p < 0.0001; unpaired two-tailed *t* test. All genotypes are listed in Supplemental Table 2.

Figure 8

Model for the Pp1 function in border cell migration. (**A**) Schematic of the phenotypes and the localizations of F-actin, p-Sqh, and the cadherin-catenin complex during normal and Pp1-inhibited (NiPp1 expression or *Pp1c-RNAi*) border cell cluster migration. (**B**) Proposed molecular pathways regulated by Pp1, which together promote cohesive collective border cell migration.

Fig 1

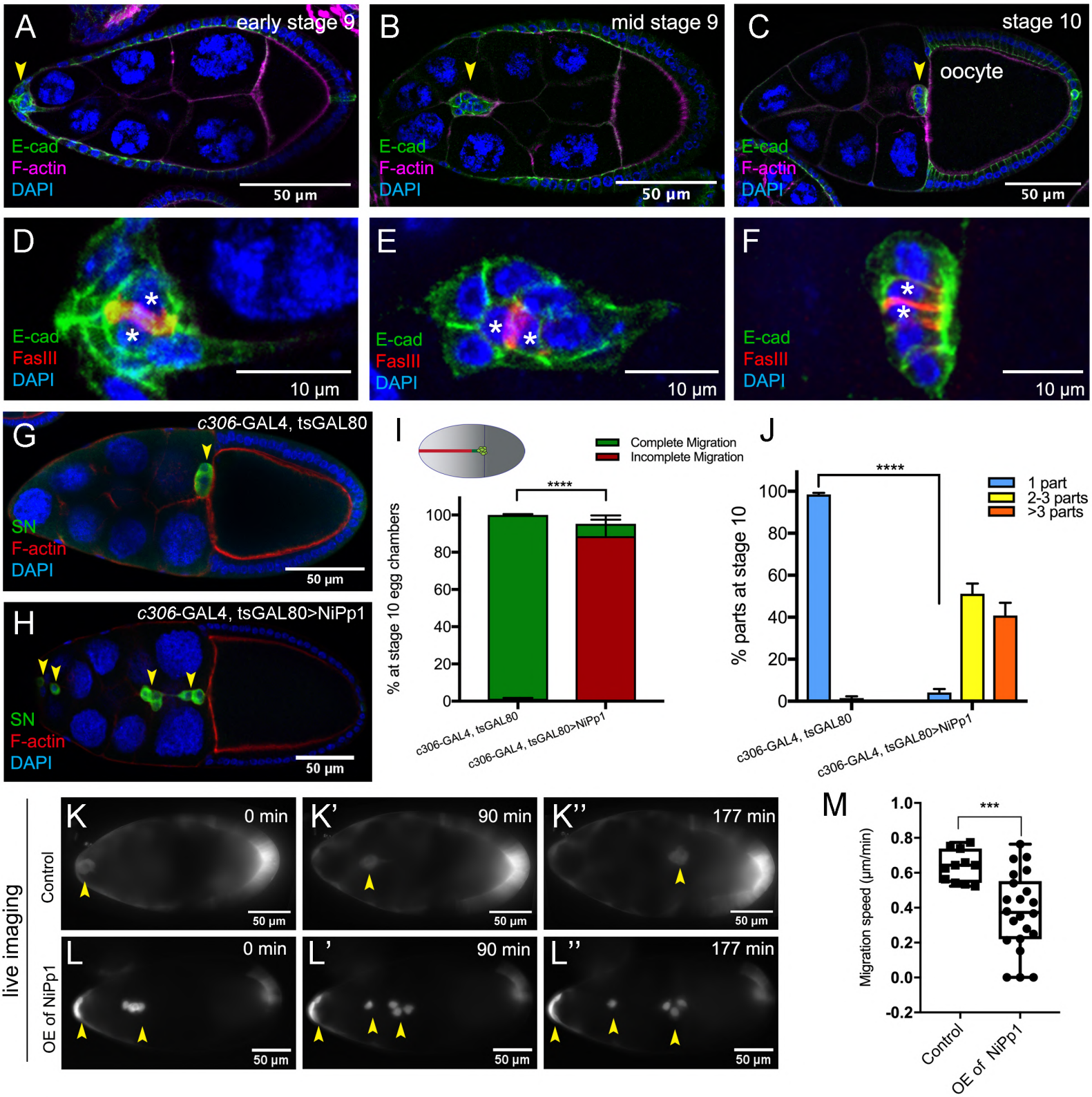

Fig 2

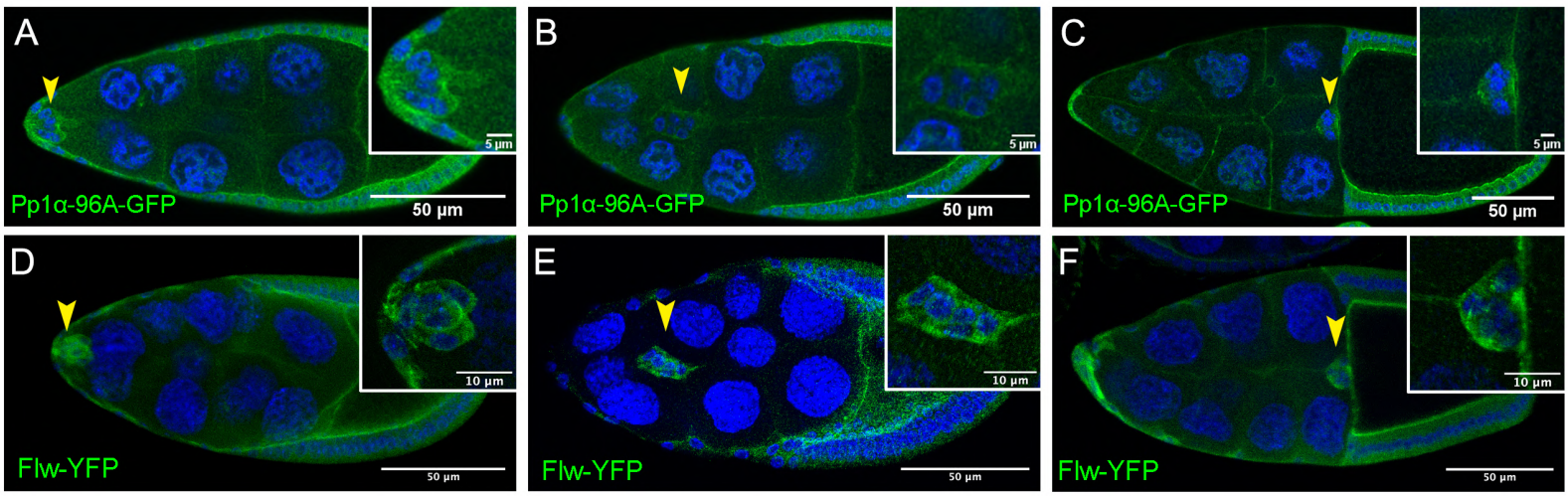

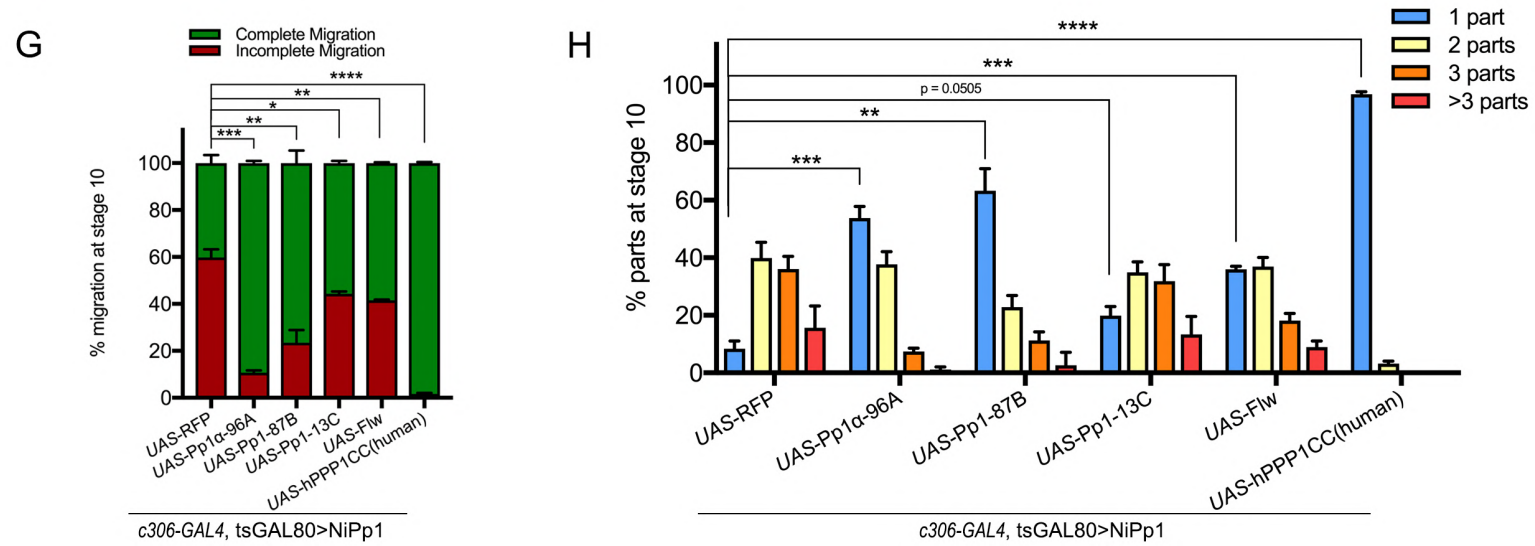

Fig 3

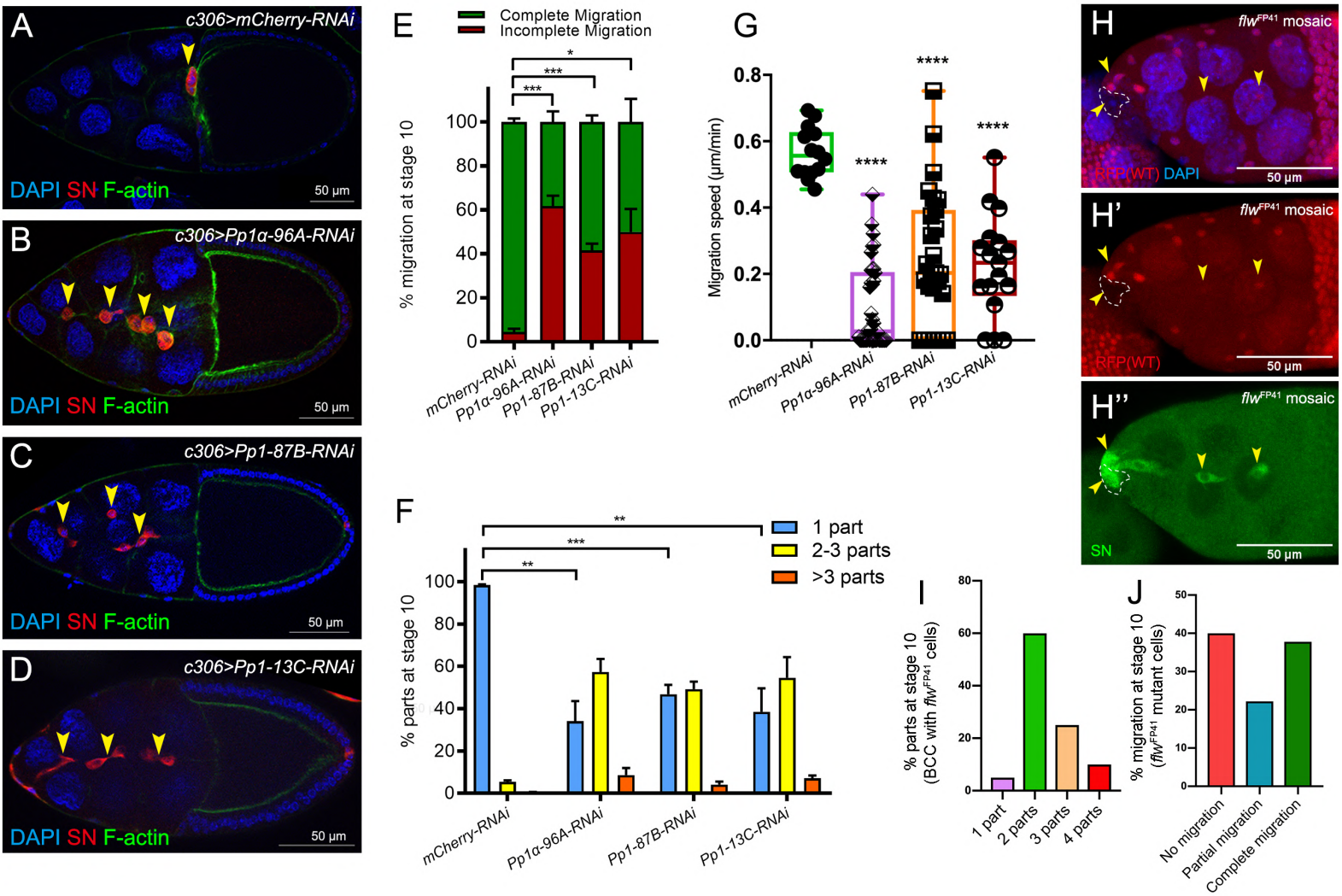

Fig 4

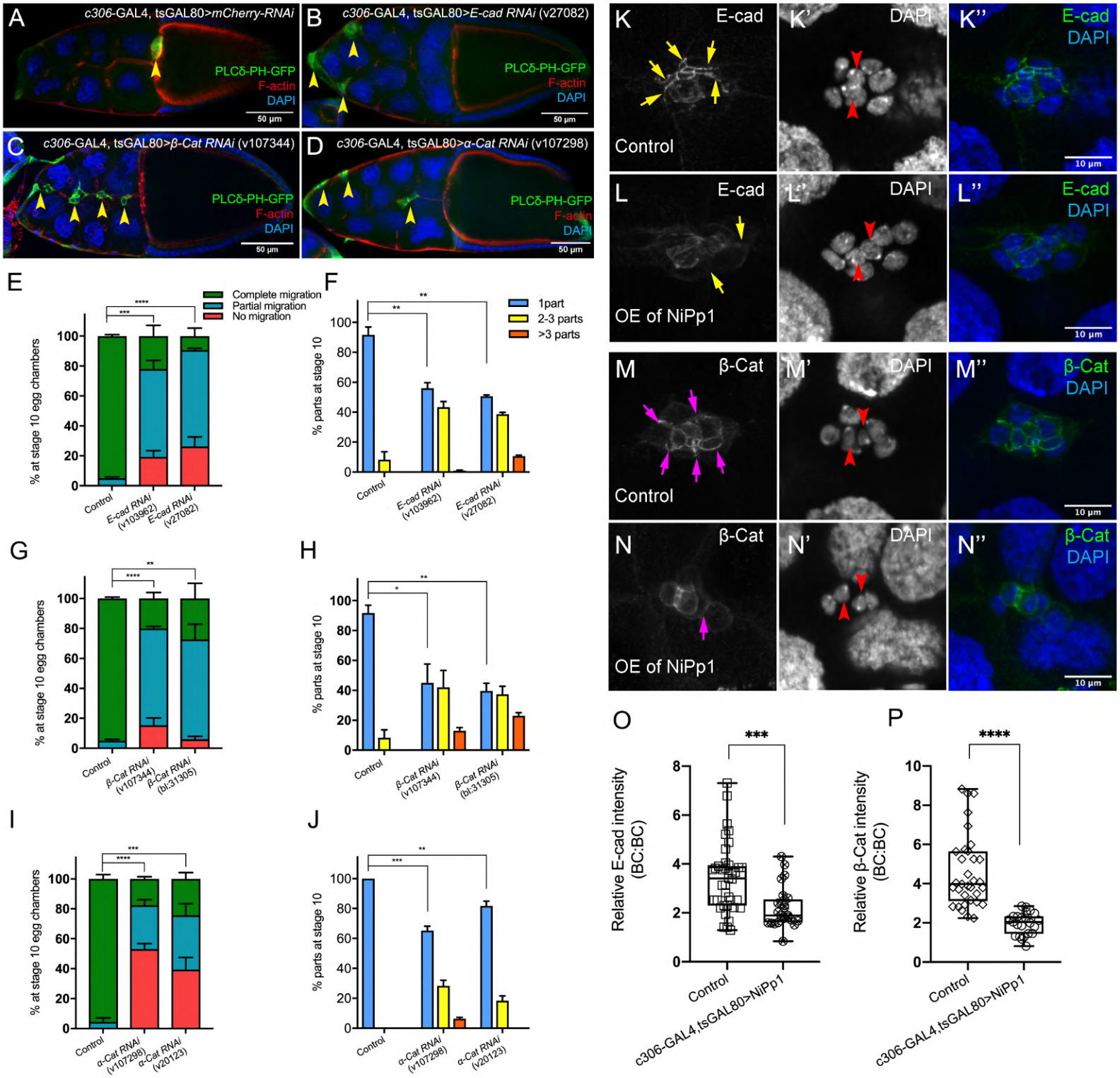

Fig 5

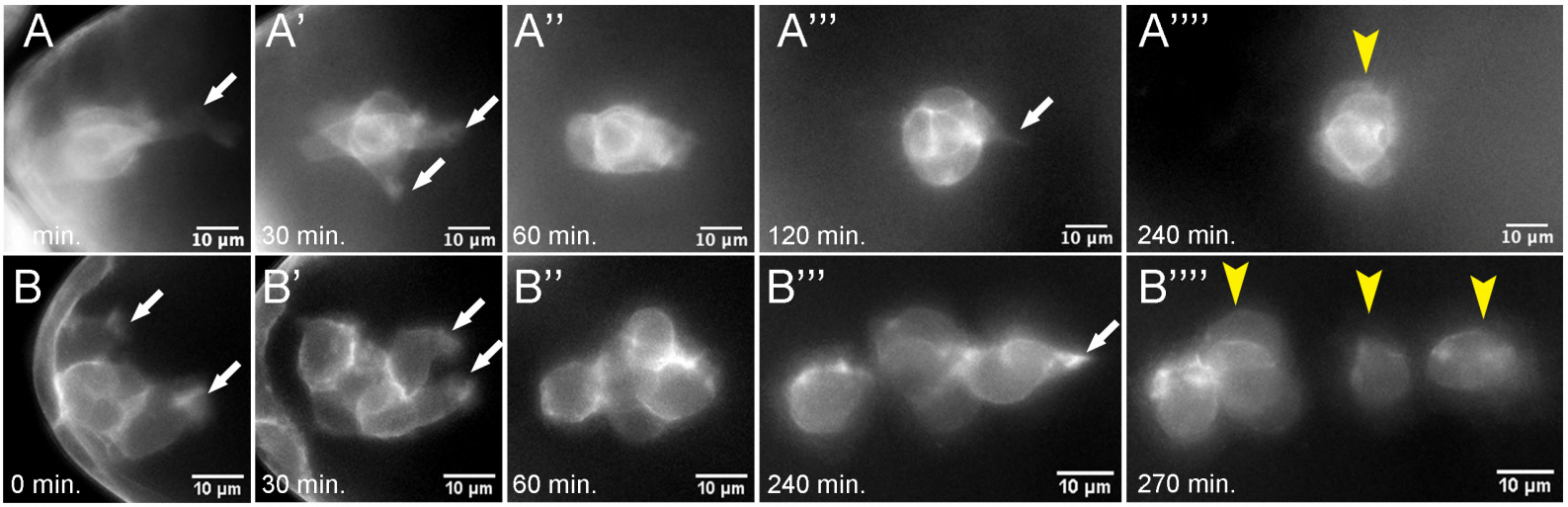

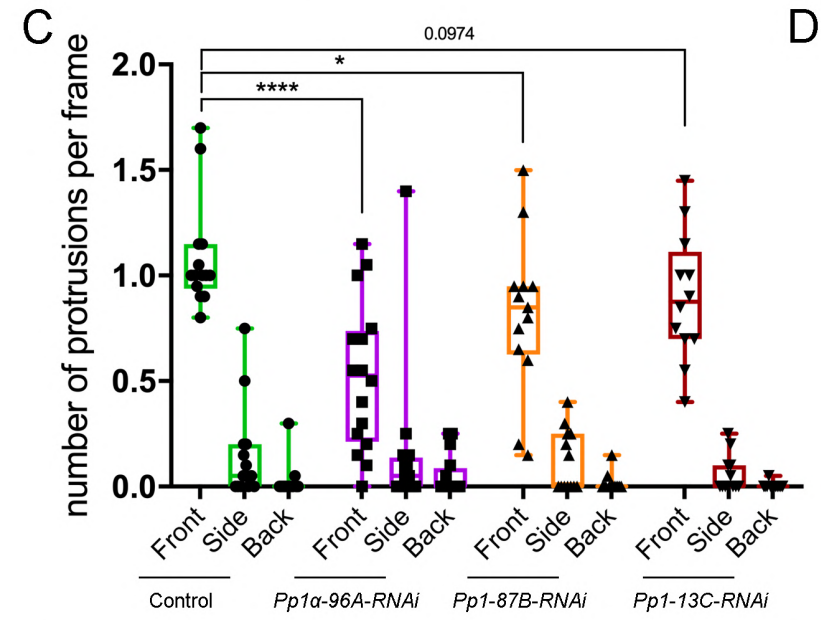

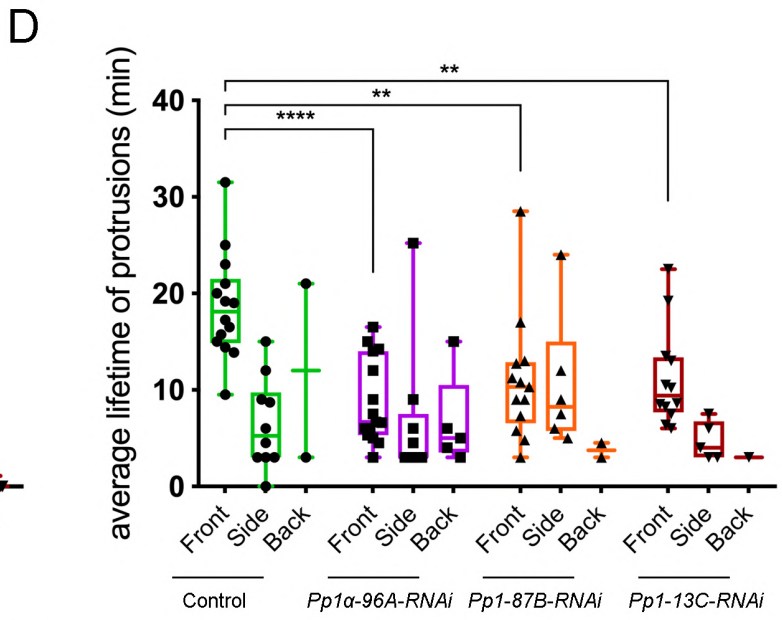

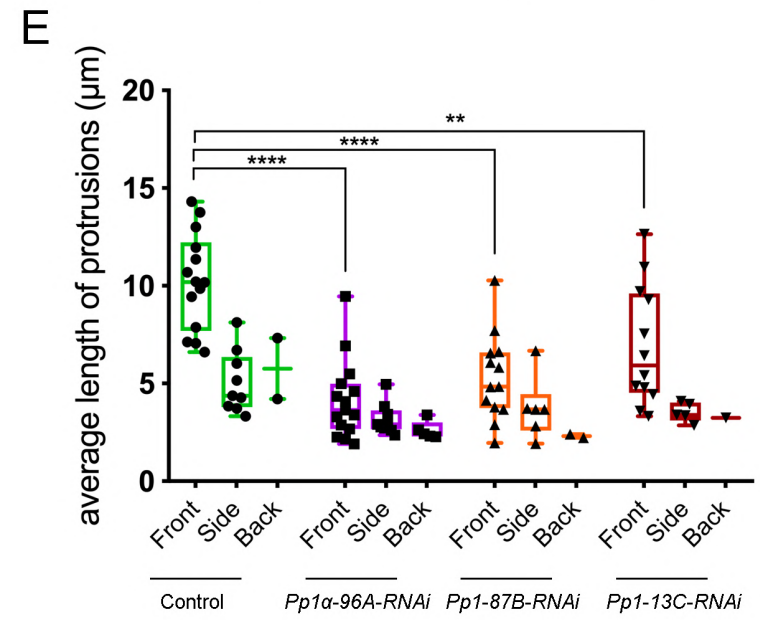

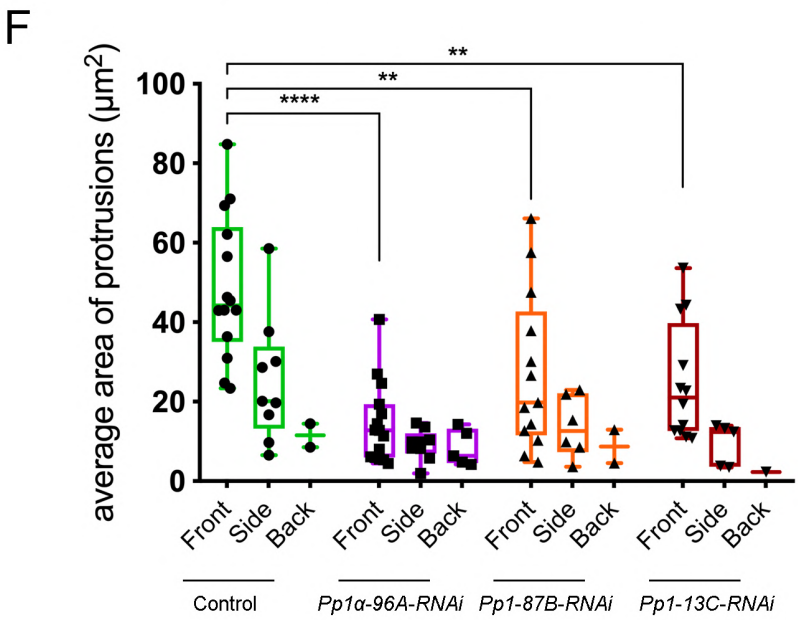

Fig 6

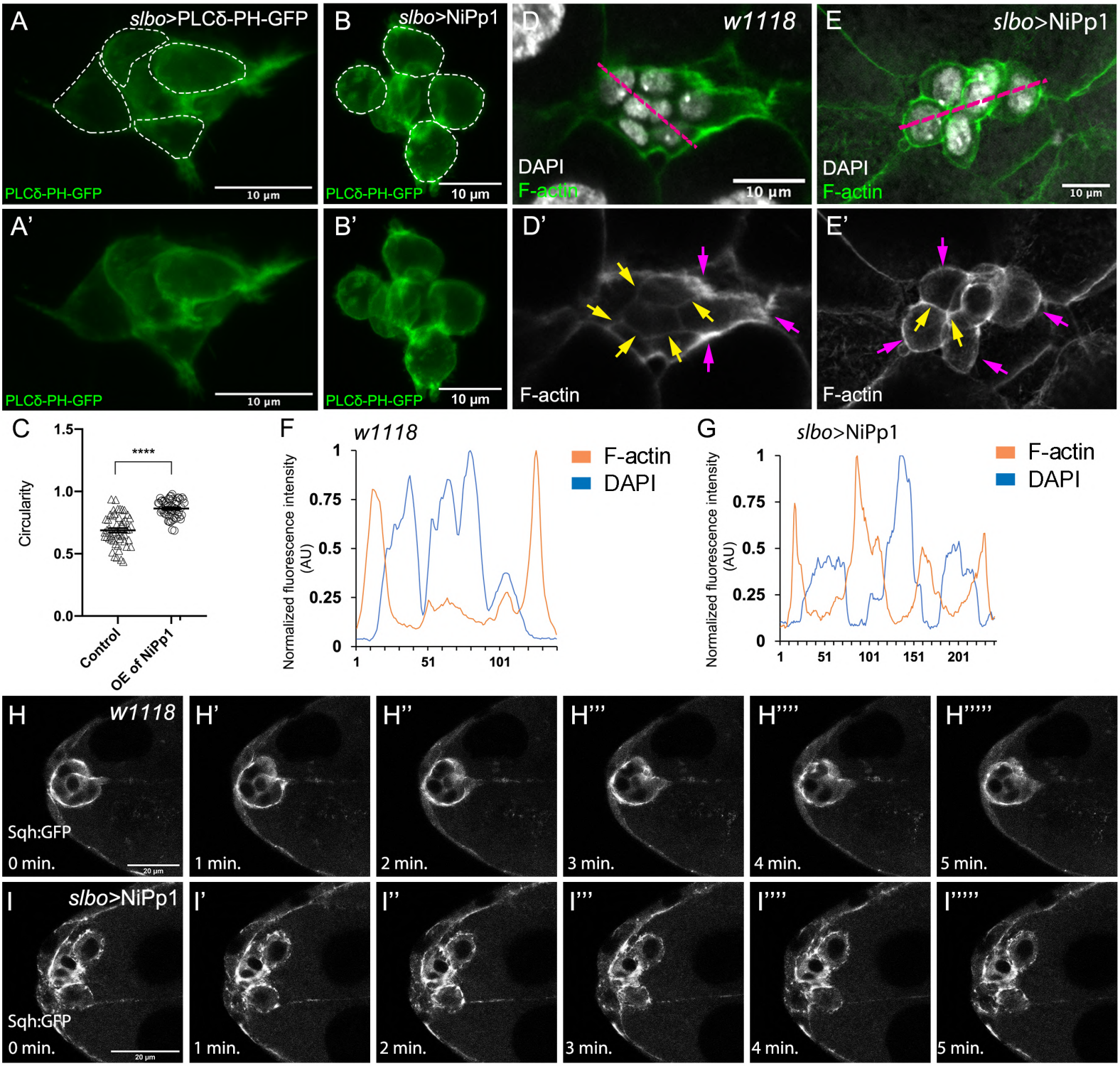

Fig 7

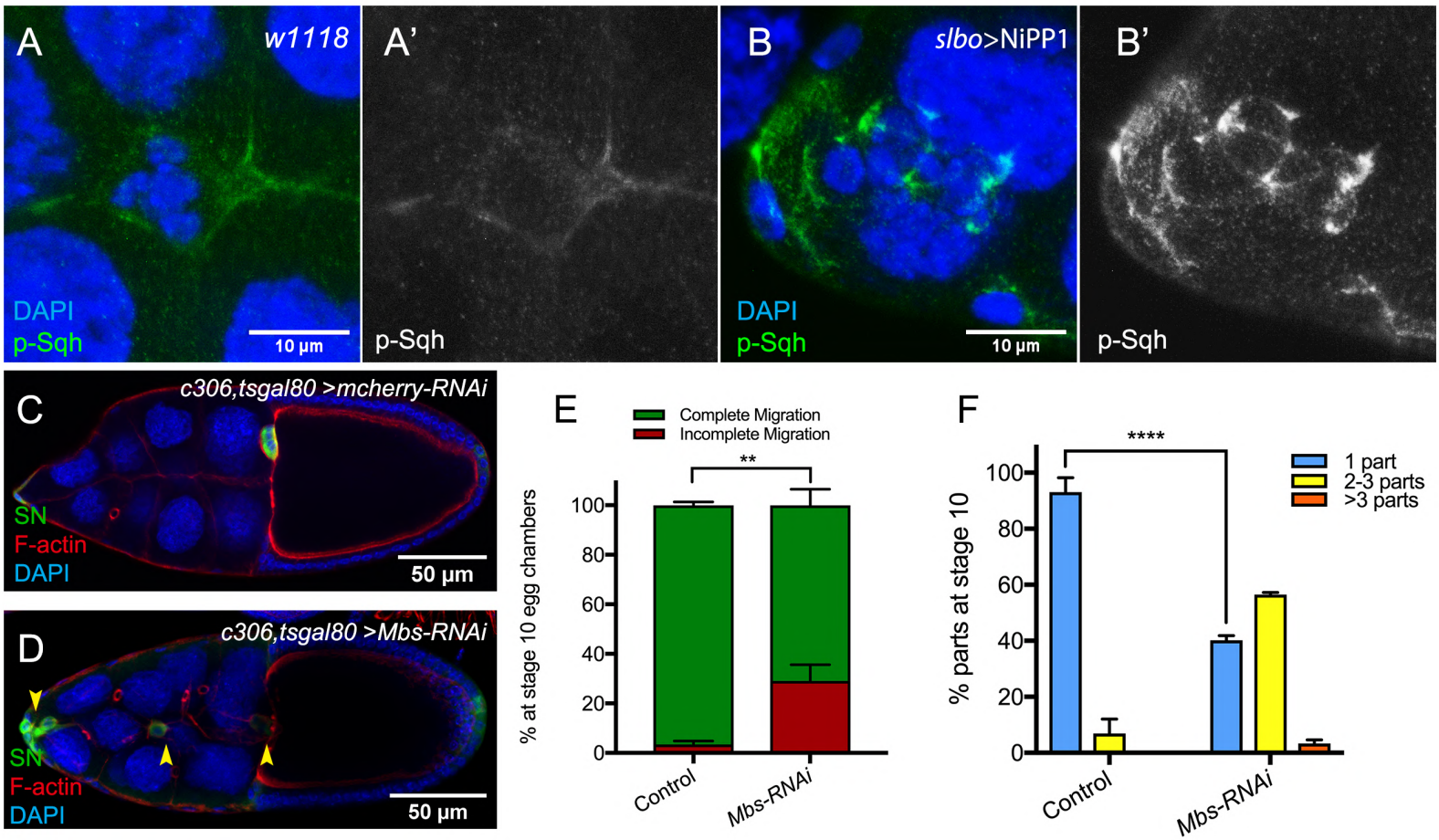

Fig 8

A

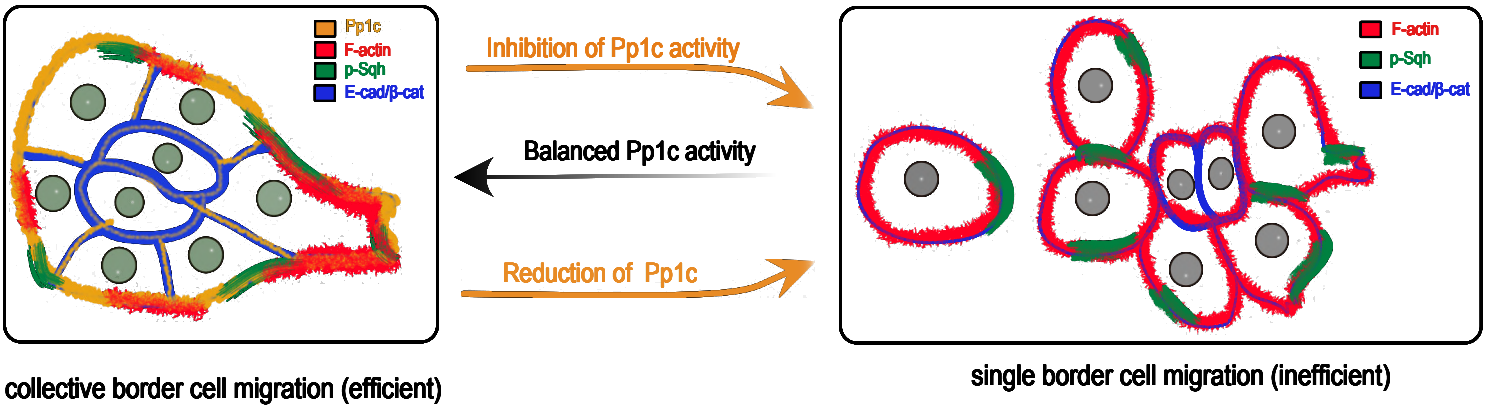

B